ERDC/CHL TR-20-19

Coastal and Hydraulics Laboratory

US Army Corps
of Engineers®
Engineer Research and
Development Center

ERDC
ENGINEER RESEARCH & DEVELOPMENT CENTER

Regional Sediment Management and Dredging Operation and Environment Research

Physical Factors That Influence Muddy Bed Aggregate Production, Size, and Durability

David W. Perkey, Kelsey A. Fall, and S. Jarrell Smith

September 2020

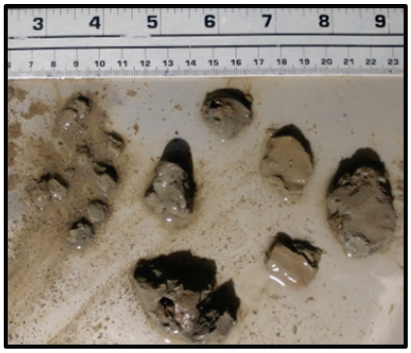

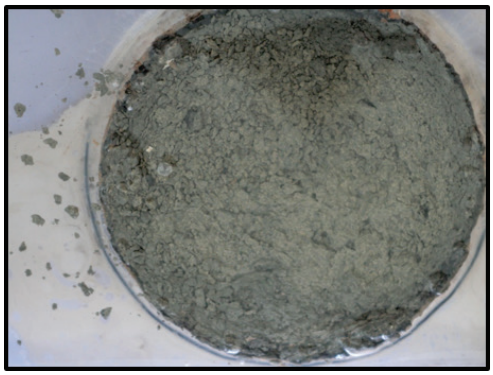

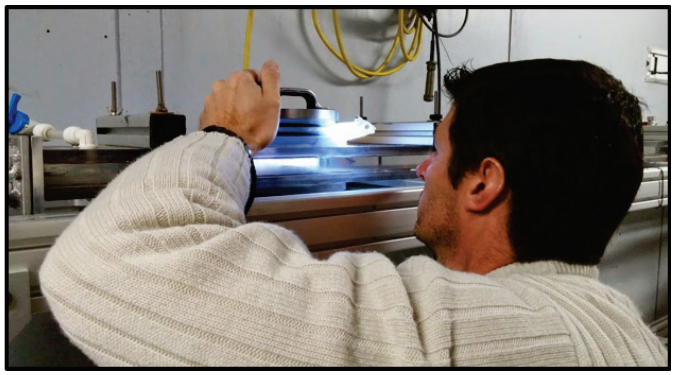

The U.S. Army Engineer Research and Development Center (ERDC) solves the nation's toughest engineering and environmental challenges. ERDC develops innovative solutions in civil and military engineering, geospatial sciences, water resources, and environmental sciences for the Army, the Department of Defense, civilian agencies, and our nation's public good. Find out more at www.erdc.usace.army.mil.

To search for other technical reports published by ERDC, visit the ERDC online library at http://acwc.sdp.sirsi.net/client/default.

ERDC/CHL TR-20-19
September 2020

Physical Factors That Influence Muddy Bed Aggregate Production, Size, and Durability

David W. Perkey, Kelsey A. Fall, and S. Jarrell Smith

Coastal and Hydraulics Laboratory
U.S. Army Engineer Research and Development Center
3909 Halls Ferry Road
Vicksburg, MS 39180-6199

Final report

Prepared for The Regional Sediment Management Program (RSM) and the Dredging Operations and Environmental Research Program (DOER) Vicksburg, MS 39180

Under RSM: “James River Federal Navigation Channel, Lower Reaches” – Account Code D15945 AMSCO 008303
DOER: “Aggregate Transport” – Account Code B3209G AMSCO 089500

Abstract

Aggregation state significantly influences the transport characteristics of fine sediments. While research has documented the presence of mud aggregates in multiple coastal and estuarine environments, bed aggregates are largely absent from numerical models used to predict cohesive sediment transport. The U.S. Army Corps of Engineers (USACE) is conducting studies to evaluate the impact muddy bed aggregates have on sediment management issues, and how to account for aggregates in numerical models.

In this study, physical properties associated with cohesive behavior were evaluated to determine if they could be used as predictors for bed aggregate production, size, and durability. Results showed that aggregates were consistently produced in cohesive sediments, and that median aggregate size was ~10-450x larger than the disaggregated sediment. Clay content had strong correlation with relative aggregate size, though statistically significant correlations were also found with sand content, water content, and density. Durability testing indicated that aggregate break-up followed exponential models, and that in limited instances, rates of break-up correlated with organic content.

Contents

Figures and Tables

Figures

Tables

Preface

This study was conducted for the Regional Sediment Management (RSM) under "James River Federal Navigation Channel, Lower Reaches" and the Dredging Operations and Environmental Research (DOER) Programs under "Aggregate Transport."

The work was performed by the Field Data Collection and Analysis Branch of the Navigation Division, U.S. Army Engineer Research and Development Center, Coastal and Hydraulics Laboratory (ERDC-CHL). At the time of publication, Mr. William Butler was Chief of the Field Data Collection and Analysis Branch; Dr. Jacqueline Pettway was Chief of the Navigation Division; and Mr. Charles E. Wiggins was the Technical Director for Navigation. The Deputy Director of ERDC-CHL was Mr. Jeffrey R. Eckstein, and the Director was Dr. Ty V. Wamsley.

The Commander of ERDC was COL Teresa A. Schlosser, and the Director was Dr. David W. Pittman.

1 Introduction

1.1 Background

Effective sediment management within the nation's navigable waterways and coastal areas is an important mission to the U.S. Army Corps of Engineers (USACE). In many instances, the sediments in these areas are mixtures of sand, silt, and clay; making their erosion and transport processes more complex than sand alone (Mehta et al. 1989; Mitchner and Torfs 1996). Research has shown that the presence of fine (<63 μm) material within the sediment matrix leads to cohesive behavior (Mitchner and Torfs 1996; Van Ledden et al. 2004; Barry et al. 2006; Jacobs et al. 2011; Dickhudt et al. 2009, 2011; Wu et al. 2018) and the production of aggregated clasts upon mobilization from the bed (Mitchner and Torfs 1996; Jepsen et al. 2010; Schieber et al. 2010; Mehta 2013, Winterwerp et al. 2012; Perkey et al. 2020). As summarized by Perkey and Smith (2019), muddy bed aggregates have been documented to occur both in the lithological record and in modern deposits across a wide range of environments. They have also been shown to frequently occur in conjunction with dredging of the consolidated sediment bed (e.g. Fettweis et al. 2009; Smith and Friedrichs 2011; Carey et al. 2013). Aggregated clasts have been shown to have settling velocities, densities, and transport pathways that are significantly different from their constituent particles (e.g. Jepsen et al. 2010; Schieber et al. 2010; Smith and Friedrichs 2011; Perkey et al. 2020). However, limited information is available regarding the physical properties that lead to the production, abundance, size, and durability of these muddy aggregates. This knowledge gap limits the capability for these types of aggregated clasts to be incorporated into sediment management studies.

Differences in transport characteristics (e.g. initiation, mode, frequency) between bed aggregates and disaggregated constituent particles have significant implications for sediment transport management. At present, many numerical models used in sediment management projects (e.g. AdH, SEDZLJ, Delft3D, ROMS) do not include aggregate properties and transport processes in their simulations, and limit the transport of fine sediment to suspended load (Brown et al. 2019; Thanh et al. 2008; Lesser et al. 2004; Delft Hydraulics 2007; Warner et al. 2008, 2010). Because these bed aggregates can significantly alter the transport and fate of fine

sediment, guidance is needed to inform the scientific and engineering community on the physical properties that result in bed aggregate production, and when it is appropriate to incorporate them into numerical sediment transport simulations.

1.2 Objective

The goal of this technical report is to identify commonly utilized physical properties of sediment that can be used to predict the production, size, and durability of muddy bed aggregates upon erosion. Predictive capabilities such as these may then be used to develop methods that allow for the incorporation of muddy bed aggregates into numerical transport models.

1.3 Approach

The production of aggregated particles upon erosion from the bed has been linked to the cohesive nature of sediment (Mitchner and Torfs 1996; Jepsen et al. 2010; Schieber et al. 2010; Mehta 2013, Winterwerp et al. 2012; Perkey et al. 2020). Sediment cohesion is commonly impacted by sediment properties such as grain size, density, water content, plasticity, volume fraction mud, and organic content (Mitchner and Torfs 1996; Jacobs et al. 2011; Dickhudt et al. 2009, 2011; Wu et al. 2018; Grant and Gust 1987; Yallop et al. 1994). Sediments from a variety of harbors, channels, and waterways from across the country were evaluated to determine if physical properties that impact cohesion could be used to predict the production of eroded bed aggregates (Figure 1). These sediments were selected due to their heterogeneous composition, wide geographic spread, and association with recently conducted USACE sediment management projects.

Figure 1. Regional map of test sediment locations.

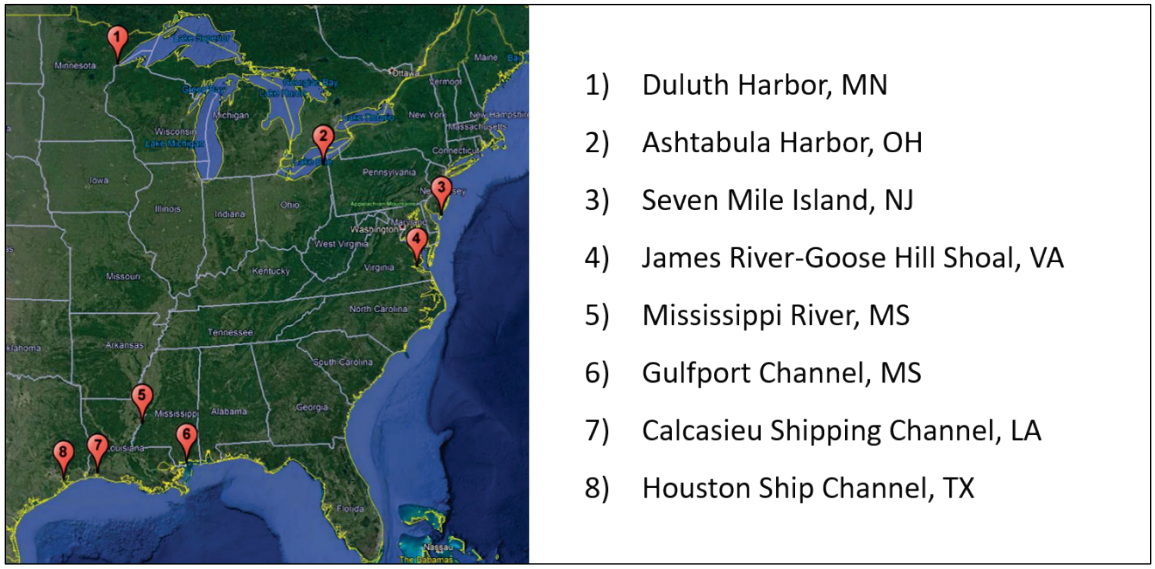

To test these materials for bed aggregate production, flume based experiments were performed with the USACE developed Sedflume (McNeil et al. 1996) coupled with the Flume Imaging Camera System (FICS) (Perkey et al. 2020; Fall et al., 2020). The occurrence and relative size of bed aggregates was determined by comparing the median grain size of eroded particles to the median grain size of the disaggregated sediment test beds. Correlations between these median grain size ratios and the various physical properties measured for each sediment were examined to assess if certain parameters were viable predictors for the presence and relative size of bed aggregates. Additionally, the durability of aggregated clasts formed from each of the test materials was characterized with a modified Slake Durability tumbling device.

2 Methods

2.1 Erosion testing

2.1.1 Sedflume

All erosion testing was performed with the USACE- developed Sedflume, which is a derivative of the flume developed by researchers at the University of California at Santa Barbara (McNeil et al. 1996). The flume includes an 80-cm-long inlet section (Figure 2) with cross-sectional area of 2 × 10 cm for uniform, fully developed, smooth-turbulent flow, as described in McNeil et al. (1996). The inlet section is followed by a test section with a 10-cm diameter open bottom. Coring tubes and flume test section, inlet section, and exit sections are constructed of clear polycarbonate materials to permit observation of sediment-water interactions during the course of erosion experiments. The flume includes a port over the test section to provide access to the core surface for physical sampling. The flume accepts sediment cores up to 80-cm in length.

Figure 2. Images of the Sedflume (upper left), erosion surface (lower left), and operator (lower center), along with operational test range of the flume (right).

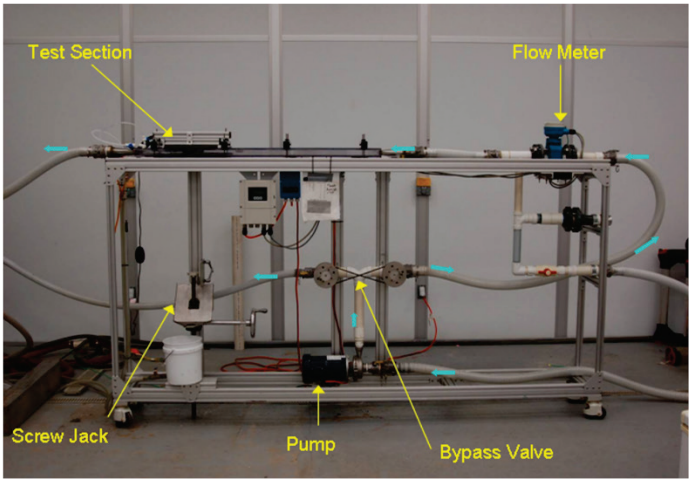

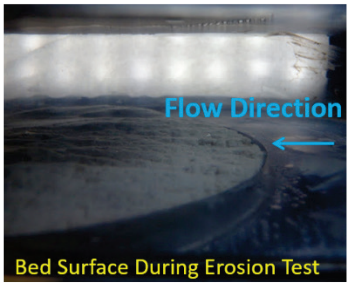

Shear Stress (Pa)	Flow Rate (GPM)
0.1	5.2
0.2	7.9
0.4	11.5
0.8	17.8
1.5	25.8
1.0	20.3
1.5	25.8
2.0	30.6
2.5	34.9
3.0	38.8
4.0	46.0
5.0	52.4
6.0	58.3
8.0	69.1
10.0	78.8
12.0	87.7

Cores are inserted into the testing section of Sedflume and a screw jack is used to advance the plunger such that the core surface becomes flush with the bottom wall of the flume. Flow is directed over the sample by diverting water from a 5.5-hp trash-pump, through a 5-cm inner diameter hose, into the flume. The flow through the flume produces shear stress on the surface of the core. Numerical, analytical, and experimental analyses have been performed to relate flow rate to bottom shear stress (Figure 2). As sediment is eroded from the core surface, the operator advances the screw jack to maintain the sediment surface flush with the bottom wall of the erosion flume. Erosion experiments are performed by repeating a sequence of increasing shear stresses. Approximately 1-5 mm of sediment is eroded at each specified shear stress; thus, the duration of each test is dependent on the rate of erosion. A diagram depicting this erosion test process along with an example erosion sequence is shown in Figure 3.

Figure 3. Diagram of sediment core erosion process. The brown arrow indicates advancement of sediment into the flume with erosion. The blue arrow indicates flow direction of water. An example erosion sequence is provided in the table to the right of the sediment core.

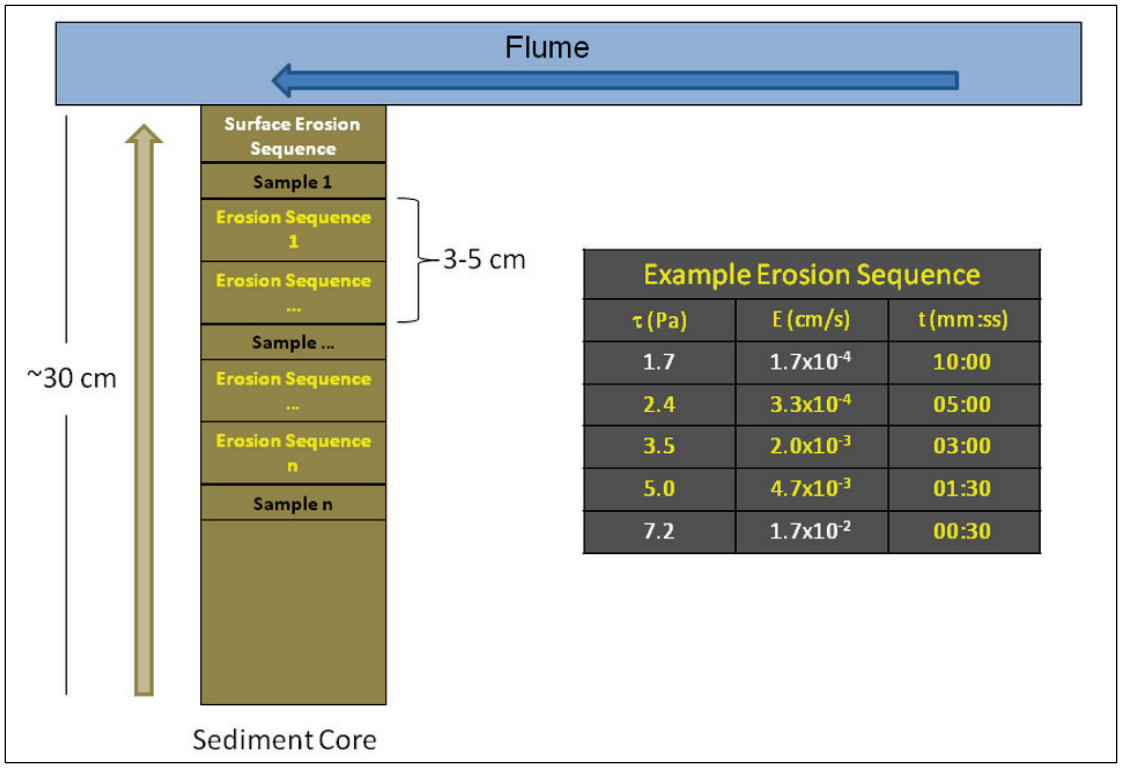

2.1.2 Eroded particle imaging

The FICS is an ERDC-developed system designed to characterize grain size distributions of sediment particles immediately following mobilization from the bed (Figure 4). The FICS consists of a clear polycarbonate channel, an Allied Vision, Manta G504B camera equipped with an Opto Engineering TC23056 bi-telecentric lens, and an Allied Vision LED back light paired with a Pulsar 320 strobe controller. The FICS channel is designed to attach directly to the outflow end of the Sedflume. It measures 22.5 cm in length and has the same 2 x 10 cm cross-sectional area as the Sedflume channel. The camera and lens are centrally mounted 12.8 cm above the top of the channel. FICS images an area of 4.5 x 5.3 cm, with a focal depth of 2.7 cm. Magnification of the system is 0.157x, resulting in a subject pixel size of ~22 μm. Videos were collected at a rate of 3 frames per second (fps), with an exposure of 500 μs and gain set to 10. The backlight was pulsed with 24V, 50 A with a pulse width of 30 μs. FICS videos had a default length of 240 frames (80 s) and were collected at every erosion interval. In cases where the erosion interval duration was less than 80 s, video collection was terminated early. For longer erosion intervals (duration exceeding 5 min), multiple videos were collected approximately every 5 min.

Figure 4. Schematic showing the FICS system mounted to the outflow end of the Sedflume.

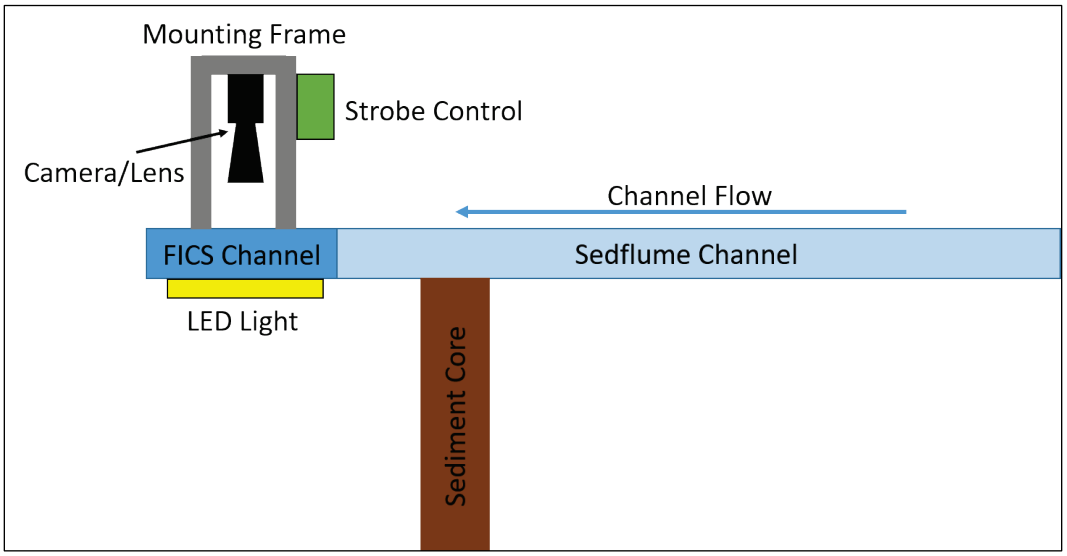

An automated image analysis routine was used to characterize the size of eroded particles in FICS images. Prior to erosion testing, a calibration grid was inserted into the FICS channel and photographed for the purpose of

transforming pixel space to length. The processing routine utilizes this gridded image and employs algorithms from the MATLAB Image Processing Toolbox. It combines local intensity thresholding with particle vetting to identify particles, while omitting unwanted features such as background objects, air bubbles, and out of focus particles. FICS image processing requires particles to appear in an area of at least 3 x 3 pixels. Therefore, the system can only accurately size particles with equivalent spherical diameters (esd) greater than approximately 66 μm.

Prior to the start of erosion testing, background FICS videos of site water were recorded to account for any sediment particles present in the water not associated with bed erosion. To analyze the imaged particles, a total of 19 equal logarithmically spaced (~1/3 ϕ) particle size bins were generated that spanned the size range of 63 μm – 16000 μm. These bin properties were used to generate a volume based particle size distribution for all the FICS videos. FICS distributions obtained from background videos were subtracted from videos recorded during erosion testing to produce a net distribution representative of eroded particles. These distributions were used to obtain the median size of eroded particles observed by the FICS (D_{50F}). Further details on these processing techniques can be found in Smith and Friedrichs (2011) and Fall et al. (2020).

2.1.3 Core preparation

The general guidelines for preparing sediment mixtures is to sufficiently homogenize the sample to minimize down-core variability of sediment properties that would otherwise affect erosion behavior. To achieve this, all sediment samples were mixed for a minimum of 30 min before transfer into 10-cm diameter polycarbonate tubes. Prior to placing sediment in the tube, a plunger with bentonite paste (for sealing and lubrication) was inserted into the bottom of the core.

Two methods were utilized to prepare cores for erosion testing. For mixtures that displayed fluid behavior, the sample was poured through a funnel and pipe, which was inserted into the core tube, allowing the sediment column to be filled from the bottom up and minimize gas entrapment. For samples with lower water contents that displayed more plastic and granular behavior, samples were tamped into the core tube in approximately 1 to 2 cm lifts. After filling the core tubes, overlying water was placed on top of the sediment column and the prepared cores were allowed to consolidate in a 4°C cooler for approximately 30 days prior to

erosion. Table 1 provides sample preparation method information for each of the cores. A brief description of each test material is provided in the following section.

Table 1. Prepared test cores.

Sample Name	Preparation Method	Location	Material Description
DH	Poured Slurry	Duluth Harbor	Dredged Sediment (Composite)
ARE45	Poured Slurry	Inner Ashtabula Harbor	Native Bottom Sediment
ARE60	Poured Slurry	Outer Ashtabula Harbor	Native Bottom Sediment
SMIIL	Poured Slurry	Seven Mile Island	Native Bottom Sediment (Composite)
JR	Poured Slurry	James River	Dredged Sediment
MS100	Poured Slurry	Mississippi River	Native Bottom Sediment
MS029	Tamped Lifts	Mississippi River	Lab Prepared Mixture
MS021	Tamped Lifts	Mississippi River	Lab Prepared Mixture
MS011	Tamped Lifts	Mississippi River	Lab Prepared Mixture
MS003	Tamped Lifts	Mississippi River	Lab Prepared Mixture
GP	Poured Slurry	Gulfport Entrance Channel	Native Bottom Sediment
CSC	Poured Slurry	Calcasieu Shipping Channel	Native Bottom Sediment (Composite)
HSC	Poured Slurry	Houston Shipping Channel	Dredged Sediment

2.2 Test sediments

In this study, a series of bottom sediments collected from multiple federal navigation channels and were evaluated for their propensity to produce aggregated clasts upon erosion. All of these sediments were held in a 4°C cooler at the Engineer Research and Development Center-Coastal and Hydraulics Laboratory (ERDC-CHL) sediment properties facility in Vicksburg, MS prior to use in this study. A map indicating the regional locations of each of the sediment types is provided in Figure 1. Samples were grouped into four classifications based on geographical setting: 1) Great Lakes Region, 2) Mid-Atlantic Coast, 3) Mississippi River, and 4) Gulf Coast. A brief description of each sediment type is provided in this section.

2.2.1 Great Lakes Region

2.2.1.1 Duluth Harbor, MN (DH)

In 2013, the USACE Detroit District (LRE) conducted a study concerning the transport potential of dredged material used for newly constructed shoals and islands within Duluth Harbor, MN. These sediments were muddy in texture with fines contents (<63 μm) ranging from approximately 55-90%. Notes from initial erosion testing indicated the presence of muddy bed aggregates produced upon erosion. Archived sediments from the 2013 experiments were composited for testing in this study.

2.2.1.2 Ashtabula Harbor, OH

Beneficial use of dredge material projects are currently being conducted by the USACE Buffalo District (LRB) within Ashtabula Harbor, OH. To characterize the sediment properties and evaluate the transport processes of dredged material following placement, bottom grab samples were collected in 2018 from the inner (ARE-45) and outer (ARE-60) regions of the harbor. Inner harbor material was muddy in texture with a fines content of ~95%, while outer harbor sediments were coarser in composition (54% sand). Both materials were used in this study.

2.2.2 Mid-Atlantic Coast

2.2.2.1 Seven Mile Island, NJ

In 2019, the USACE Philadelphia District (NAP) launched the Seven Mile Island Innovation Laboratory (SMIIL) to advance and improve dredge material management and marsh restoration techniques in coastal New Jersey. Sediments from the proposed dredging area within the New Jersey Intracoastal Waterway were collected. Samples from the channel were found to be composed of approximately 60% fines and 40% sand.

2.2.2.2 James River, VA (JR)

The USACE Norfolk District (NAO) is conducting a series of sediment management studies in the James River, VA in an effort to improve the understanding of impacts associated with existing dredge material placement strategies within the system. In 2017, bottom sediments were collected from the Goose Hill Shoal placement area and shipped to the

ERDC-CHL for Sedflume erosion testing. Sediments from the upstream portion of the shoal had fines contents of approximately 80% and initial erosion testing notes indicated the presence of muddy bed aggregates upon erosion. Archived material from the upriver portions of the shoal were utilized for further erosion and bed aggregate testing in this study.

2.2.3 Mississippi River

Mud from a perched boat basin off the Mississippi River near Grand Gulf, MS was collected by ERDC-CHL in 2014 for use in a study to evaluate relationships between mud content and erosion thresholds. To achieve this, a series of sand-mud mixtures were prepared with known amounts of Mississippi River mud and fine silica sand (Wu et al. 2018). Five of the archived mixtures from this study had adequate remaining volumes for further testing in this study. These samples were mixtures composed of 3%, 11%, 21%, 29%, and 100% Mississippi River bottom material (MS003, MS011, MS021, MS029, and MS100, respectively).

2.2.4 Gulf Coast

2.2.4.1 Gulfport, MS (GP)

Bottom sediments were obtained from portions of the Gulfport, MS navigation channel in 2012 as part of an investigation to evaluate the impacts of fluid mud on nautical depth in the region. Collected samples had a fines content of 97%. Subsamples of these archived sediments were used in this study.

2.2.4.2 Calcasieu Shipping Channel, LA

In 2019, the USACE New Orleans District (MVN) conducted a regional sediment management study in the Calcasieu Shipping Channel (CSC), LA to investigate the sources of channel shoaling. As part of that study, bottom drag samples were collected from stretches of the navigation channel. Channel sediments were found to be muddy in texture (~70-90% fines). A composite sample was prepared and tested in this study.

2.2.4.3 Houston Shipping Channel, TX (HSC)

Newly placed dredged material from the Houston Shipping Channel was collected from a wetland restoration project being conducted by the USACE Galveston District (SWG) near Atkinson Island, TX in 2018.

Samples were found to be stiff muds composed of 99% fines. Composite slurries of this sediment were prepared and evaluated in this study.

2.3 Physical properties

Sub-samples of each sediment type were set aside for the purpose of Atterberg Limit and organic content analysis before the preparation of sediment cores. Additional physical samples for bulk sediment property measurements were taken at periodic intervals during Sedflume testing, generally at the end of an erosion cycle (Figure 3). These samples were collected by draining the flume channel, opening the port over the test section, and extracting a sample from the sediment bed. Samples collected in this manner were used to characterize the bulk density, disaggregated grain-size distribution, and volume fraction mud of the test bed. The methods used to determine these properties are presented in this section.

2.3.1 Plasticity Index

The Plasticity Index (PI) of each material was obtained through standard Atterberg Limit testing. Standard methods, described in ASTM D4318 (2015), were utilized to measure the liquid and plastic limits. To obtain the liquid limit, the multipoint method was utilized with a motorized device to maintain a constant drop rate. Plastic limit testing was conducted on a polished granite counter top using the hand method. The difference between the two limits yields the PI for each sample, which indicates the breadth of moisture content for which the material behaves plastically.

2.3.2 Organic content

To evaluate the total, volatile organic content of the sediment samples, loss on ignition (LOI) techniques described in ASTM D2974, method C (2014) were used. Following recommendations reported by Schumacher (2002) and Salehi et al. (2011), combustion temperature was reduced from 440° C down to 360° C.

2.3.3 Water content and bulk density

Water content (w) of each sample was measured through wet-dry weight analysis following ASTM D2216-19 (2019) in which w is given by

$$w = \left(\frac{m_w - m_d}{m_d} \right) \quad (1)$$

where m_w and m_d are the wet and dry weights, respectively. The total volume of sample was assumed to consist of both solid particles and water, with assumed densities of 2.65 g/cm^3 and 1.0 g/cm^3, respectively. The bulk density as a function of w and the densities of the sediment particles (ρ_s) and water (ρ_w) was calculated with equation 2, derived from Jepsen et al. (2010).

$$\rho = \rho_s + \frac{w\rho_s \left(\rho_w - \rho_s \right)}{\rho_w + w\rho_s} \quad (2)$$

2.3.4 Grain size

Grain size distributions and characterizations were obtained through Laser Diffraction Particle Size Analysis (LDPSA) with a Malvern Mastersizer 2000, which measures particle sizes in terms of equivalent spherical diameters (esd) between the range of 0.02 to 2000 μm. Sediments were homogenized and disaggregated overnight in a solution of sodium metaphosphate (40 g/L). To remove macro organic material, samples were passed through a 1000 μm sieve into the instrument's reservoir and sonicated for 60 sec prior to analysis. Median grain size (D_{50L}) was reported and the Wentworth scale (1929) was used for the classification of sand (>63 μm), silt (63-4 μm), and clay (<4 μm) sized particles.

2.3.5 Volume fraction mud

The water content, bulk density, and LDPSA grain size methods previously described were utilized to calculate the volume fraction mud (ϕ_{sm}) for test material. The equation used for calculating ϕ_{sm} follows methods described in Dickhudt et al. (2009, 2011),

$$\phi_{sm} = \frac{\phi_{stot} - f_s \phi_{stot}}{1 - f_s \phi_{stot}} \quad (3)$$

in which ϕ_{stot} is the total solids volume fraction, and f_s is the fraction sand of the sample.

2.4 Aggregate durability

To evaluate the durability of mud aggregates, a Slake Durability tumbler was utilized. This tumbler is a device that consists of a steel mesh drum (14 cm dia.) that is partially immersed and rotated at a speed of 20 rpm within a water bath. The apparatus is designed for the testing of shales and similar weak rock fragments. A detailed description of the device can be found in ASTM D4644 (1998). For the purposes of evaluating bed aggregates in this study, the standard 2 mm wire mesh of the rotating drum was replaced with 250 μm mesh.

For each sample, cube-like aggregates of ~1 cm^3 volume were prepared by extruding and slicing test material from cores or molds (Figure 5a). When possible, this was done using the remaining material following erosion testing. In some instances, water content of the eroded material was too high to allow for slicing. In these cases, w was reduced through an iterative process until a content was reached that allowed for slicing and aggregate preparation. These samples are indicated with an asterisk (*) in Table 5. Typically 3-5 aggregates were utilized for each durability test (Figure 5b). Aggregates were tumbled at intervals of 2.5, 5, 10, and 20 min (Figure 5c), which roughly correspond to linear tumbling distances of 25 m, 50 m, 100 m, and 200 m, respectively. At the completion of each test interval, the drum was removed from the water bath and the remaining contents >250 μm were filtered through pre-weighed, 90-mm diameter glass fiber filters with retention rating of 0.7 μm. Similarly, the contents of the water basin (<250μm) were filtered through pre-weighed 142 mm diameter glass fiber filters with retention rating of 0.7 μm. Filters were dried in a 50° C oven overnight before obtaining final dry masses of fractions >250 μm and <250 μm.

Standard wet sieving techniques were used on an aliquot of each test material to assess the mass fraction >250 μm prior to aggregate durability testing (ASTM D6913 2009). This fraction was subtracted from the mass fraction retained within the tumbler basket to yield a net mass fraction >250 μm ($F_{Ma\ >250}$) due to the aggregated state of the sediment.

Figure 5. Prepared mud aggregates (a) placed in test drum, (b) and tumbled in water bath, (c) for durability testing.

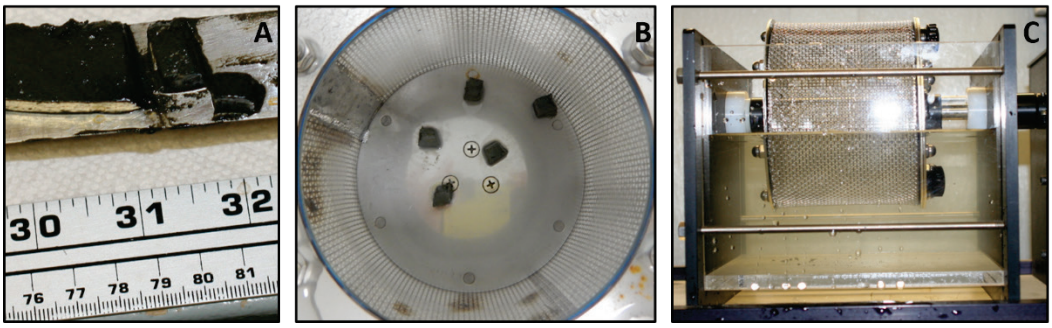

3 Results

3.1 Physical properties of test materials

The results of the physical parameters measured for each test material are presented in this section. A brief description of the findings obtained for each parameter is presented first, followed by the summarization of all physical property data in Table 2.

Table 2. Physical properties of tested sediments. Shaded cells identify samples with sand content >50%.

Sample Name	PI	% LOI	ρ (g/cm³)	w	D_{50L} (μm)	% Sand	% Silt	% Clay	ϕ_{sm}
DH	30.5	3.4	1.52	0.83	24.6	31.3	60.7	8.0	0.2
ARE45	25.6	3.1	1.48	0.91	12.7	30.6	63.8	5.6	0.3
ARE60	N/A	1.0	1.80	0.40	77.2	85.1	13.5	1.4	0.3
SMIIL	36.6	3.9	1.40	1.18	39.2	40.9	52.7	6.4	0.2
JR	59.9	4.5	1.37	1.31	15.7	18.1	68.7	13.2	0.2
MS100	49.4	3.5	1.46	0.97	10.9	3.0	80.9	16.1	0.3
MS029	8.0	N/A	1.91	0.31	136.7	78.1	18.1	3.8	0.2
MS021	N/A	N/A	2.01	0.24	146.4	85.1	12.3	2.6	0.2
MS011	N/A	N/A	2.07	0.21	155.3	92.4	6.0	1.6	0.1
MS003	N/A	N/A	2.01	0.24	161.5	99.9	0.1	0.0	0.0
GP	83.0	4.6	1.23	2.33	9.9	1.2	82.0	14.7	0.1
CSC	48.1	2.9	1.35	1.38	44.5	43.9	46.4	9.7	0.1
HSC	43.7	0.4	1.38	1.28	6.1	0.3	67.6	32.1	0.2

3.1.1 Plasticity Index

Atterberg limit testing showed that nine (9) of the thirteen (13) test samples displayed plastic behavior. The PI values of these samples ranged from 8.0-83.0, with the 29% Mississippi River sediment mixture (MS029) having the lowest PI and the Gulfport entrance channel sediment (GP) showing the highest value. Plastic behavior was not observed for the Mississippi River sediment mixtures with mud content below 29% (MS021, MS011, and MS003) or the outer Ashtabula Harbor sample

(ARE60). Therefore, no PI value could be reported for these materials. PI results for each material are presented in Table 2.

3.1.2 Organic content

Organic content measurements through LOI techniques were carried out on nine (9) of the thirteen (13) test samples. Due to limited amounts of archived test material, LOI measurements were not performed on the four laboratory prepared mixtures of Mississippi River mud and silica test sand (MS029, MS021, MS011, MS003). LOI values ranged from 0.4% -4.6%, with the Houston Ship Channel (HSC) sediment having the lowest LOI and the GP sediment showing the highest organic content. A complete listing of the LOI results is presented in Table 2.

3.1.3 Water content and bulk density

Wet-dry analyses of the test sediments showed that w ranged from 0.2-2.3 and corresponding bulk densities ranged from 1.2 – 2.1 g/cm^3. As shown in equation 2, ρ and w are inversely related, such that samples with the lowest w have the highest bulk density values. The GP sediment was found to have the highest w and lowest ρ, while MS011 had the lowest w and highest ρ. A complete listing of the water content and density results is presented in Table 2.

3.1.4 LDPSA grain size

Grain size analysis performed on the disaggregated bed samples showed that most of the sediment beds in this study were muddy in texture, with a fines content greater than 50% (Table 2). The sandy samples in the study were limited to the four laboratory prepared sand-mud mixtures made with the Mississippi River sediment, and ARE60, as identified by shading in Table 2. Sand contents of these five samples ranged from 78.1% - 99.9%. It is worthwhile to note that while the ARE60 sediment was found to be sandy (54%) in texture prior to erosion testing, bed samples collected during erosion testing showed an elevated sand contents of 85% (Table 2). This change is due to the separation of sand and fines that occurred during the 30 days of consolidation prior to erosion testing. A visible (~2 cm thick) layer of fine grain mud was present at the surface of the ARE60 core. This layer was removed prior to erosion testing so that down core changes in sediment texture did not influence erosion testing results. Bed

samples collected below the surface 2 cm showed a consistent sand content of ~85%.

LDPSA grain size distribution plots revealed that the sands in all samples were largely limited to grains <500 μm in size (Figures 6-9). MS003 was shown to have the highest sand content and coarsest median grain size (D_{50L}) at 99.9% and 161.5 μm, respectively (Table 2). However, grain size distribution plots showed that ARE60 and CSC contained the coarsest sands, with 7.6% and 3.6% of these sediments ≥500 μm, respectively. Grains > 1 mm were rarely observed in any of the sediments (Figures 6-9).

Figure 6. LDPSA distribution plots of Great Lakes Region samples from Duluth and Ashtabula Harbors.

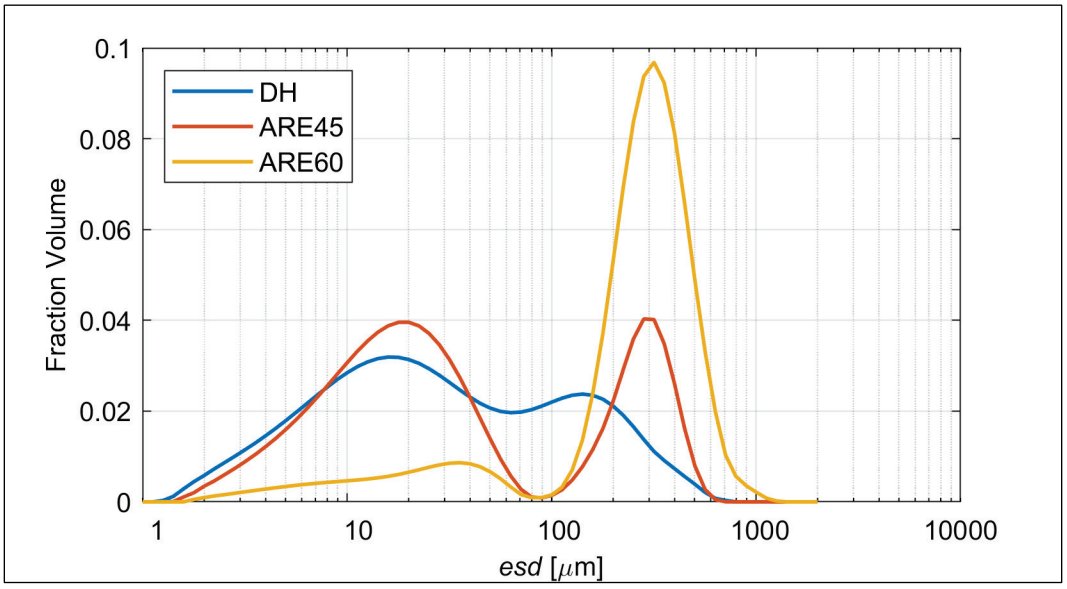

Figure 7. LDPSA distribution plots of Mid Atlantic Coast samples from Seven Mile Island and James River.

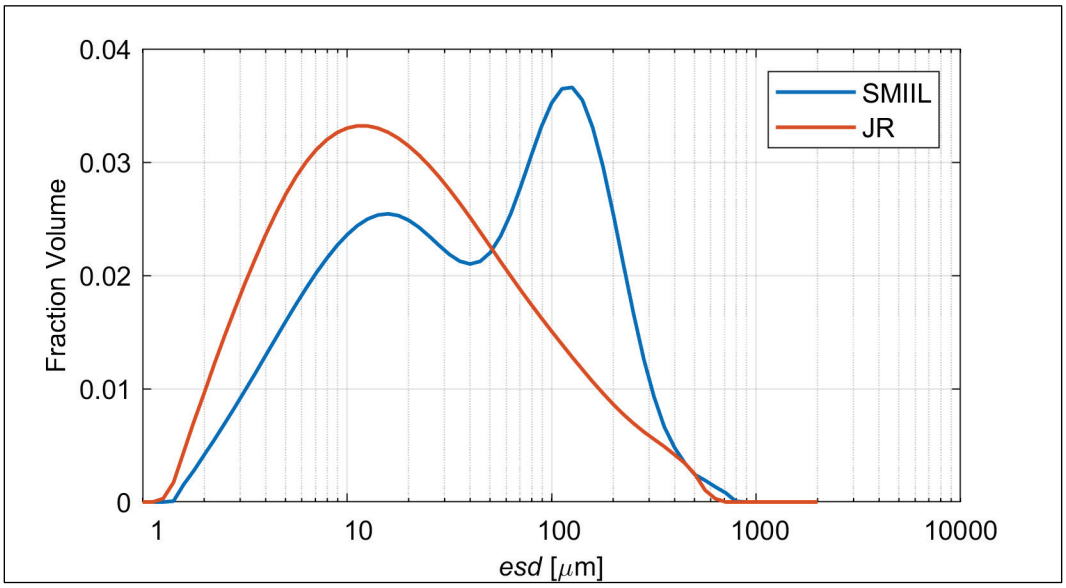

Figure 8. LDPSA distribution plots of Mississippi River sediment mixtures.

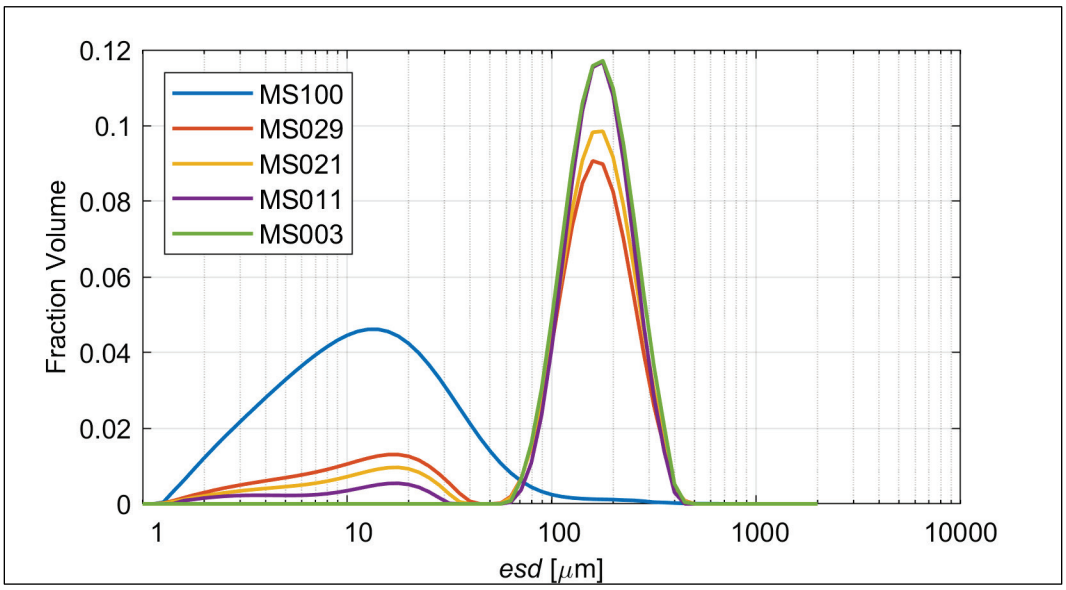

Figure 9. LDPSA distribution plots of Gulf Coast samples from Gulfport, Calcasieu Ship Channel, and Houston Ship Channel.

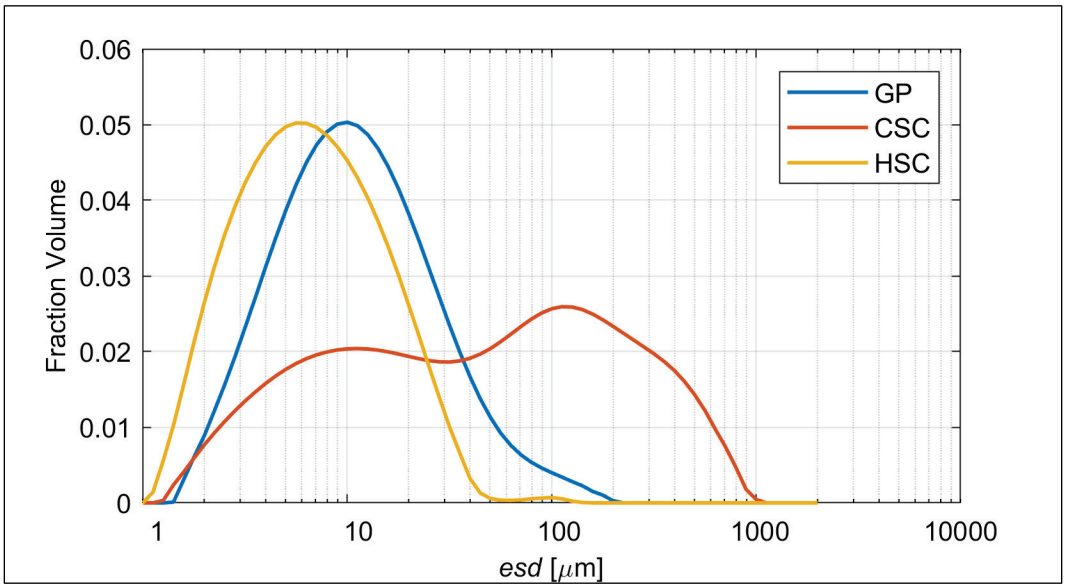

3.1.5 Volume fraction mud

Use of the LDPSA sand data, along with the wet-dry analyses data, allowed for the calculation of the ϕ_{sm} for each sediment type in the study. These values ranged from 0.0-0.3. Sample MS003 had a small mud content (0.1%) producing a very small ϕ_{sm} value reported as 0.0 in Table 2. The two Ashtabula Harbor samples (ARE45 and ARE60) along with the 100% Mississippi River sediment showed the highest ϕ_{sm} values of 0.3.

3.2 Erosion tests

3.2.1 Eroded particle size

Sedflume erosion tests were conducted within the upper 10 cm of each core at shear stresses that ranged from 0.3 Pa – 7.4 Pa (Table 3). Visual observations and notes consistently indicated the mobilization of aggregated clasts from the sediment beds. Descriptions of cloudy water downstream of the erosion surface and winnowing of fine sediments from the bed were limited to tests conducted on sample MS003.

Table 3. Erosion test conditions and FICS median grain size (D_{50F}).

Sample Name	Depth Range (cm)	Shear Stress Range (Pa)	D_{50F} (μm)	D_{50F}/D_{50L}
DH	0-3	1.0-2.5	2170	88
ARE45	3-8	0.2-1.3	4070	320
ARE60	2-7.5	0.5-1.9	260	3.4
SMIIL	0-4	0.4-4.6	1470	38
JR	0-7.5	1.2-4.8	3850	250
MS100	0-3	0.9-3.4	2990	270
MS029	0-5	3.5-7.4	3010	22
MS021	0-3	1.0-6.3	2790	19
MS011	0-2	0.7-3.4	1500	10
MS003	0.5-3	0.3-1.1	220	1.4
GP	0-4	1.0-3.6	4440	450
CSC	0-7.5	1.2-3.1	2180	49
HSC	0-4.5	0.9-3.2	1720	280

FICS data from each erosion test showed median particle sizes on the order of hundreds of microns to several millimeters (Figure 10). Robust linear regression analysis showed a weak (R^2=0.22, $p<0.001$) positive correlation between D_{50F} and shear stress. Similarly, weak correlations were observed in FICS data collected in a field study within the James River Estuary, though statistical significance ($p<0.05$) of the correlation was limited to shear stresses ≤2 Pa (Perkey et al. 2020).

Figure 10. FICS median particle size (μm) from all erosion tests plotted against shear stress (Pa). Solid line presents robust linear regression best fit, with R^2 and p values provided. The dashed lines present the 95% confidence intervals of the fit.

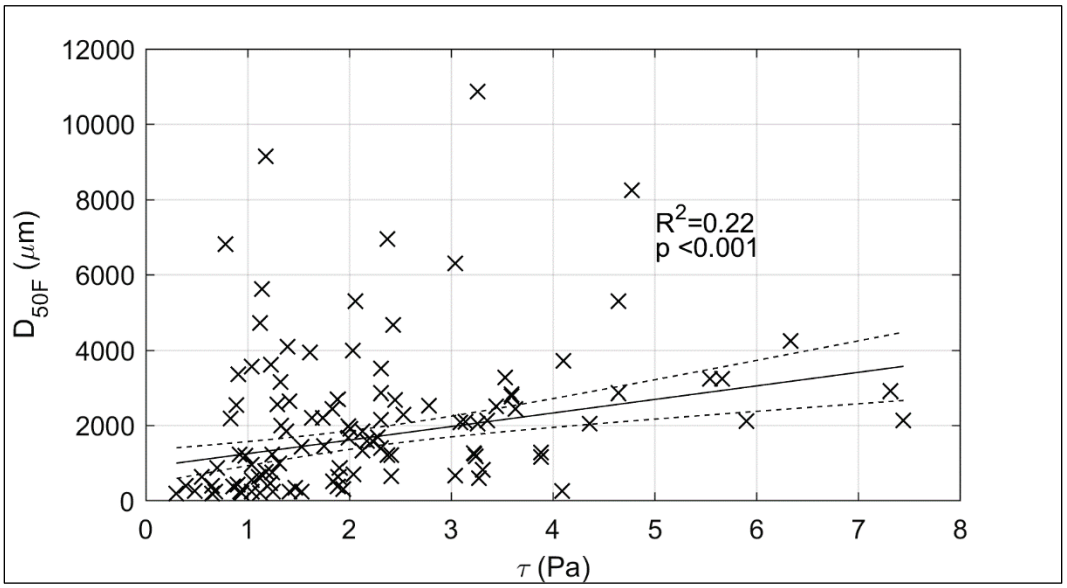

Because strong correlations were not observed between eroded particle size and shear stress, FICS videos across all shear stresses were compiled for each material, and corresponding grain size distributions were generated (Figures 11-14). The abundance of millimeter sized particles observed by the FICS is in contrast to the LDPSA size distributions obtained from the disaggregated bed samples. The compiled FICS distributions for each material showed median size to range from approximately 200 μm to 4400 μm, and in all but two cases (ARE60 and MS003), D_{50F} values were greater than 1000 μm (Table 3). A comparison of the median particle sizes obtained via FICS and LDPSA (D_{50F}/D_{50L}) revealed that the median size of eroded particles were 1.4-450x larger than median sizes of the disaggregated test beds (Table 3). In all but two instances (ARE60 and MS003), the D_{50F}/D_{50L} values in this study were ≥10. This fact further supports the visual observations made during Sedflume testing; erosion of the sediment beds predominately occurred in the form of aggregated clasts.

Figure 11. FICS distribution plots of Great Lakes Region samples from Duluth and Ashtabula Harbors.

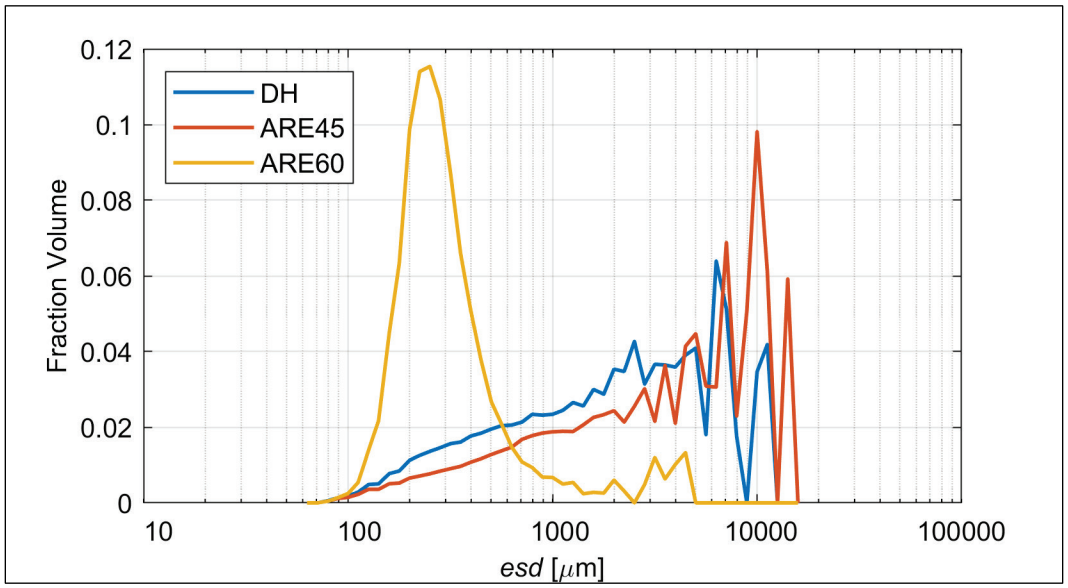

Figure 12. FICS distribution plots of Mid Atlantic Coast samples from Seven Mile Island and James River.

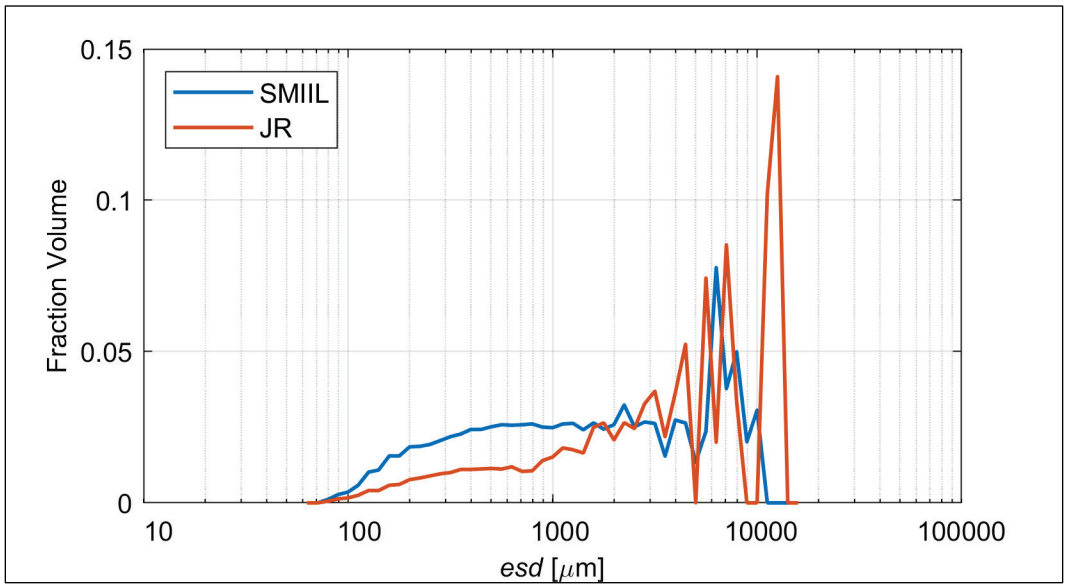

Figure 13. FICS distribution plots of Mississippi River sediment mixtures.

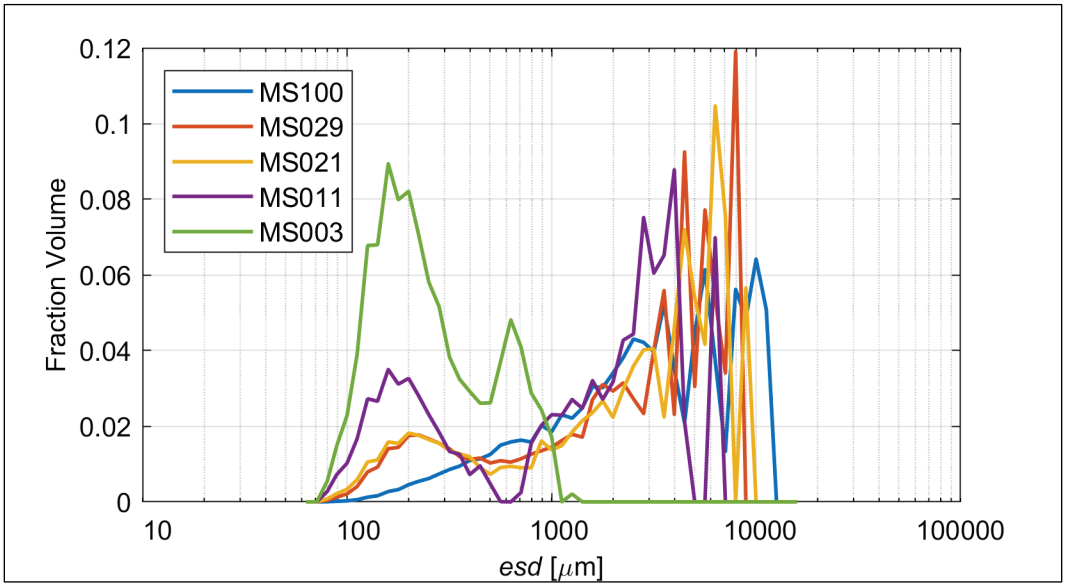

Figure 14. FICS distribution plots of Gulf Coast Samples from Gulfport, Calcasieu Ship Channel, and Houston Ship Channel.

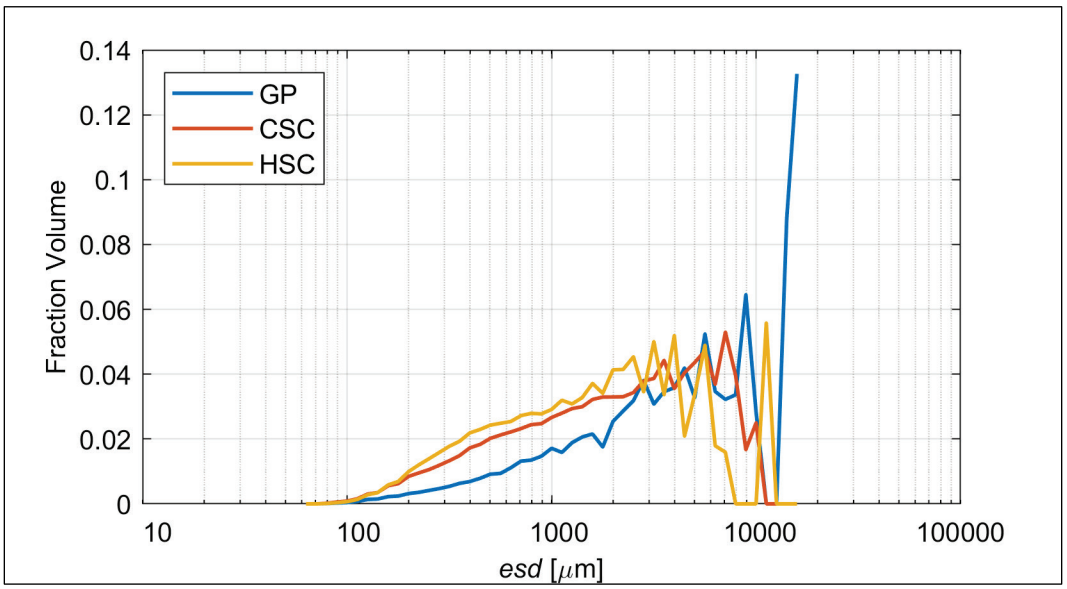

3.2.2 Regression analyses

To evaluate if physical parameters of the test sediments could be used as predictors of mud aggregate production and size, correlations between D_{50F}/D_{50L} and sediment physical properties were assessed. Robust linear regression models were determined to be statistically significant if p-values were ≤0.05. Statistically significant correlations were identified between D_{50F}/D_{50L} and clay content, sand content, w, and ρ (Table 4). Regression results showed that, of these parameters, clay content had the

highest correlation to D_{50F}/D_{50L} with $R^2 = 0.82$ and $p<0.001$ (Figure 15 and Table 4). No statistically significant correlation was found in models that plotted D_{50F}/D_{50L} against PI, ϕ_{sm}, or LOI (Table 4). Plots of these regression models are presented in Appendix A.

Table 4. D_{50F}/D_{50L} Robust liner regression model outputs. Red font indicates variable p-values >0.05 and not statistically significant to the model.

Physical Parameter	R^2	p-value(s)
%Clay	0.82	$2.2x10^{-5}$
%Sand	0.63	0.001
w	0.63	0.001
ρ	0.48	0.009
PI	0.40	0.07
ϕ_{sm}	0.10	0.30
LOI	0.07	0.49

Figure 15. Median particle size ratios plotted against clay content. Solid line presents the robust linear regression best fit, with R^2 and p values provided. The dashed lines present the 95% confidence intervals of the fit.

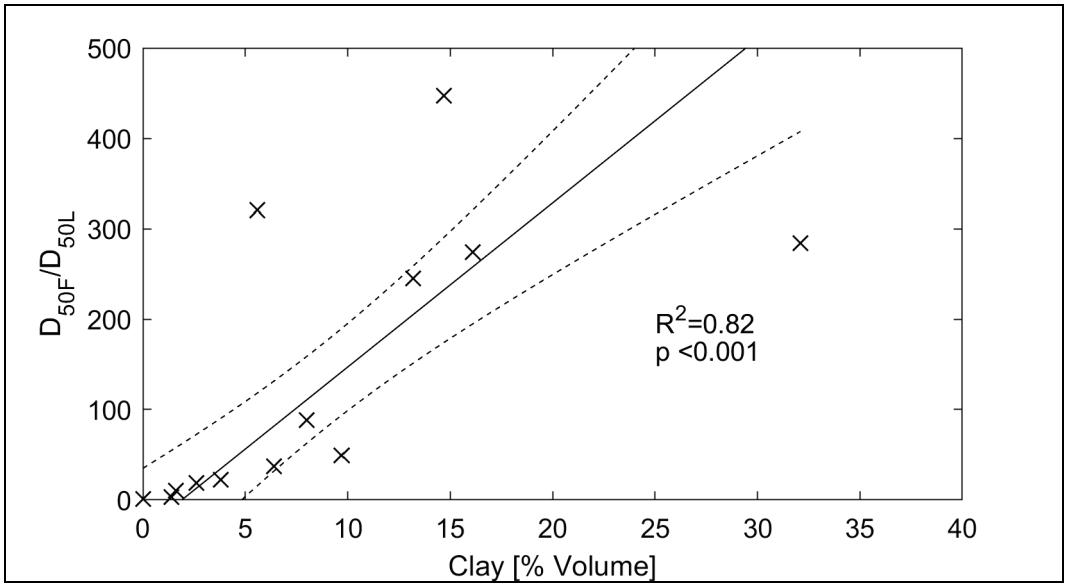

Numerous multivariate linear regression models were also run that examined correlations between D_{50F}/D_{50L} and multiple physical parameters (Appendix A). It should be noted that because an inverse relationship exists between *w* and ρ, as seen in equation 2, regression models with both these parameters were not run. Results of the multi-

variable linear regressions showed that only the model using PI and ϕ_{sm} showed statistically significant correlation to D_{50F}/D_{50L}, as indicated by the asterisk in Table 5. However, with an R^2 value of 0.7, this regression model does not account for as much variance in the D_{50F}/D_{50L} data as clay content alone. Further, materials that displayed no plastic behavior such as MS021 and MS011 both had D_{50F}/D_{50L} values ≥10 (Tables 2 and 3), suggesting that aggregated clasts were produced during erosion. Therefore, PI may not be the most appropriate parameter to use in predicting aggregate production and size.

Table 5. D_{50F}/D_{50L} Multiple liner regression model outputs presented in ascending R^2 values. * indicates model with all p-values ≤0.05. Red font indicates variable p-values >0.05 and not statistically significant to the models.

Parameters	R^2	p-value(s)
PI, ϕ_{sm}	0.70	0.01, 0.05 *
%Clay, %Sand, PI, LOI	0.82	0.20, 0.07, 0.31, 0.29
%Clay, %Sand, PI, ϕ_{sm}, LOI	0.82	0.41, 0.54, 0.61, 0.90, 0.41
w, PI, ϕ_{sm}	0.85	0.09, 0.97, 0.01
%Clay, %Sand, *w*, PI, LOI	0.85	0.43, 0.13, 0.59, 0.94, 0.63
%Clay, *w*, PI, ϕ_{sm}	0.86	0.99, 0.14, 0.97, 0.03
%Sand, *w*, PI, ϕ_{sm}	0.89	0.36, 0.08, 0.55, 0.04
w, ϕ_{sm}, LOI	0.91	0.001, 0.003, 0.48
%Sand, ρ, PI, ϕ_{sm}, LOI	0.94	0.97, 0.12, 0.92, 0.13, 0.59
ρ, ϕ_{sm}, LOI	0.95	0.001, 0.004, 0.40
ρ, PI, ϕ_{sm}, LOI	0.95	0.04, 0.86, 0.01, 0.31
%Clay, %Sand, *w*, ϕ_{sm}, LOI	0.95	0.88, 0.61, 0.03, 0.06, 0.98
%Clay, %Sand, ρ, PI, LOI	0.95	0.73, 0.04, 0.13, 0.84, 0.99
%Clay, *w*, PI, ϕ_{sm}, LOI	0.95	0.96, 0.12, 0.97, 0.04, 0.94
%Clay, ρ, PI, ϕ_{sm}, LOI	0.95	0.73, 0.13, 0.84, 0.04, 0.99
%Clay, %Sand, ρ, PI, ϕ_{sm}, LOI	0.95	0.71, 0.75, 0.37, 0.97, 0.49, 0.87
%Clay, %Sand, *w*, PI, ϕ_{sm}	0.96	0.12, 0.08, 0.03, 0.15, 0.02
w, PI, ϕ_{sm}, LOI	0.96	0.03, 0.83, 0.01, 0.92
%Sand, *w*, PI, ϕ_{sm}, LOI	0.96	0.74, 0.09, 0.71, 0.11, 0.82
%Clay, %Sand, *w*, PI, ϕ_{sm}, LOI	0.99	0.32, 0.31, 0.15, 0.84, 0.17, 0.36

While several other multivariable regression models accounted for as much or more variance as clay ($R^2 \geq 0.82$), none of them had associated p-values for each variable that was ≤0.05 (Table 5). This indicated that not all the properties were statistically significant to the model at a 95% confidence level, and therefore these results were not considered to be significant improvements over the single variable regression models.

3.3 Durability

Tumbling testing showed that the durability of the aggregates varied considerably across the test materials, as shown in Figures 16-19. MS003 was found to be the least durable with no detectable aggregated mass after 2.5 minutes of testing, thus, it was not plotted in Figure 18. MS011 and ARE60 also broke apart quickly and had no detectable mass within the tumbler basket following 5 min of testing. Because of this, no trend lines are plotted for these samples in Figures 16 and 18. The remaining ten samples all showed break-up rates that closely followed an exponential model with $R^2 > 0.88$ and p-values <0.02 (Table 6). In these models, the aggregated mass fraction >250 μm is related to tumbling time (t) through the abrasion rate (δ) shown in equation 4:

$$F_{Ma>250} = Ae^{-\delta t} \tag{4}$$

While aggregate abrasion closely matched an exponential model, the deterioration rate varied substantially, as seen in δ in Table 6. Only seven of the test samples had measurable aggregated mass in the tumbler after 20 min. Of these, only four had $F_{Ma>250}$ greater than 0.1 (MS029, JR, GP, and HSC; Figures 16-18). Aggregates from MS029 material were by far the most robust with $F_{Ma>250} = 0.44$ after 20 min of tumbling (Figure 17) and a δ of 0.042 (Table 6).

Figure 16. Aggregate durability plots of Great Lakes Region samples from Duluth and Ashtabula Harbors. Dotted lines indicate exponential fits with associated R^2 values.

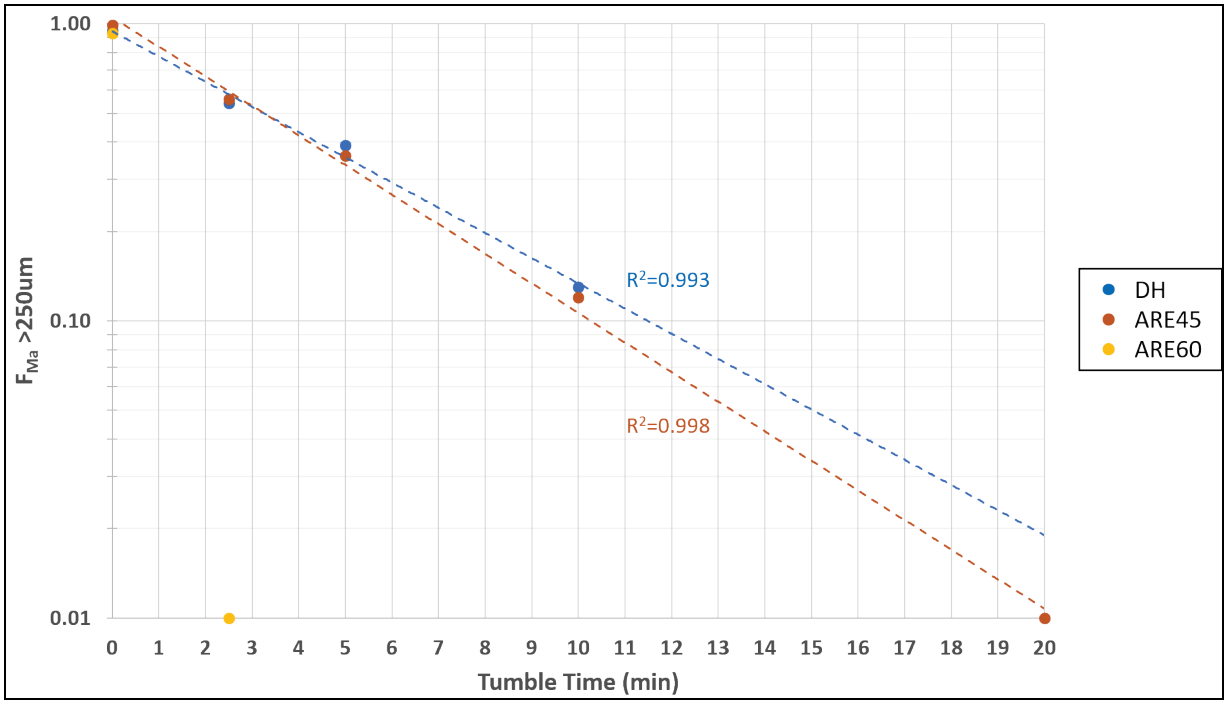

Figure 17. Aggregate durability plots of Mid Atlantic Coast samples from Seven Mile Island and James River. Dotted lines indicate exponential fits with associated R^2 values.

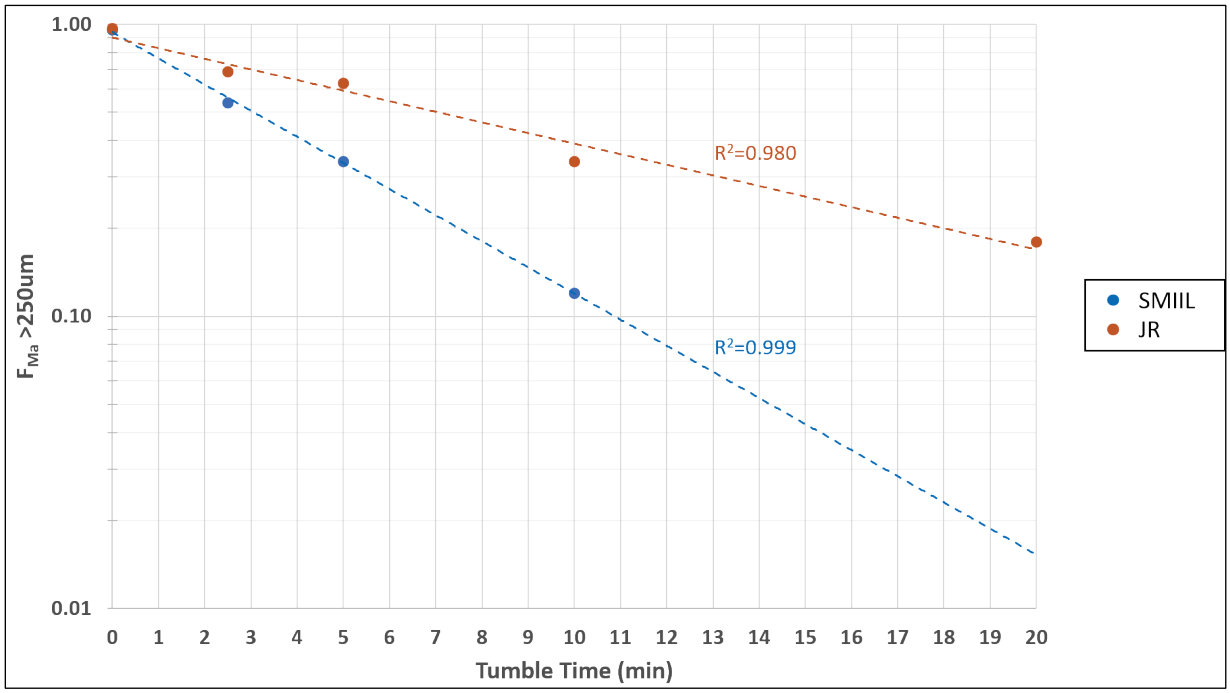

Figure 18. Aggregate durability plots of Mississippi River sediment mixtures. Dotted lines indicate exponential fits with associated R^2 values.

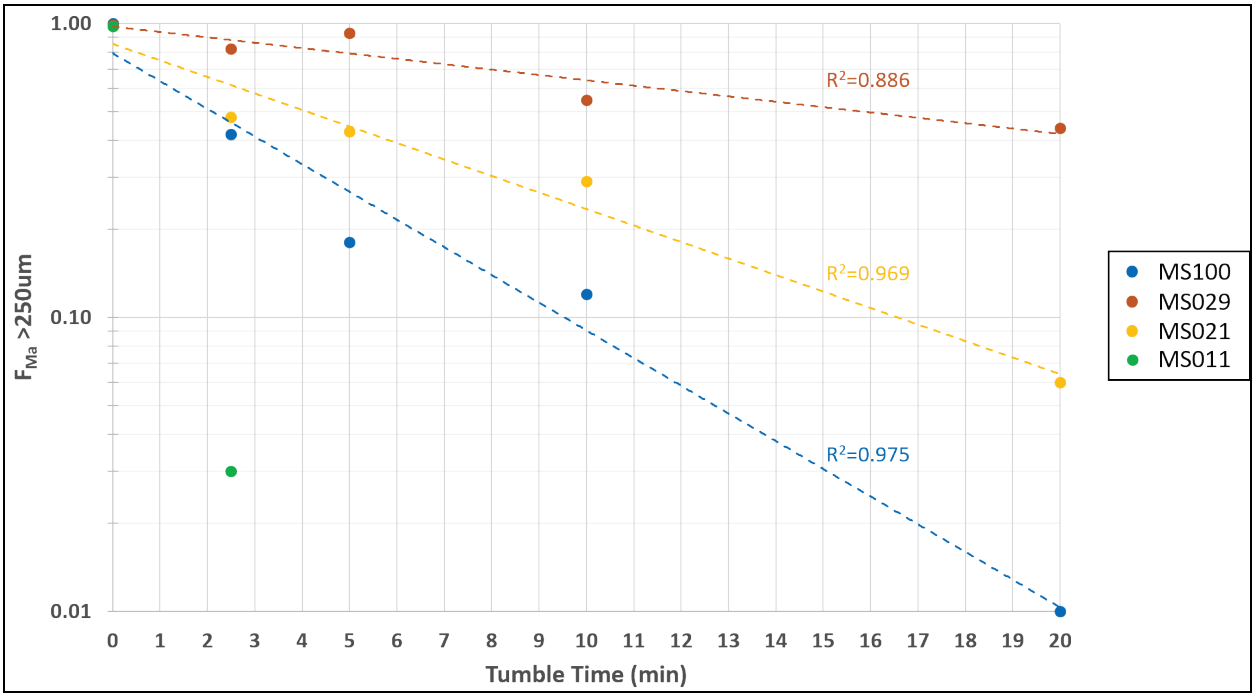

Figure 19. Aggregate durability plots of Gulf Coast samples from Gulfport, Calcasieu Ship Channel, and Houston Ship Channel. Dotted lines indicate exponential fits with associated R^2 values.

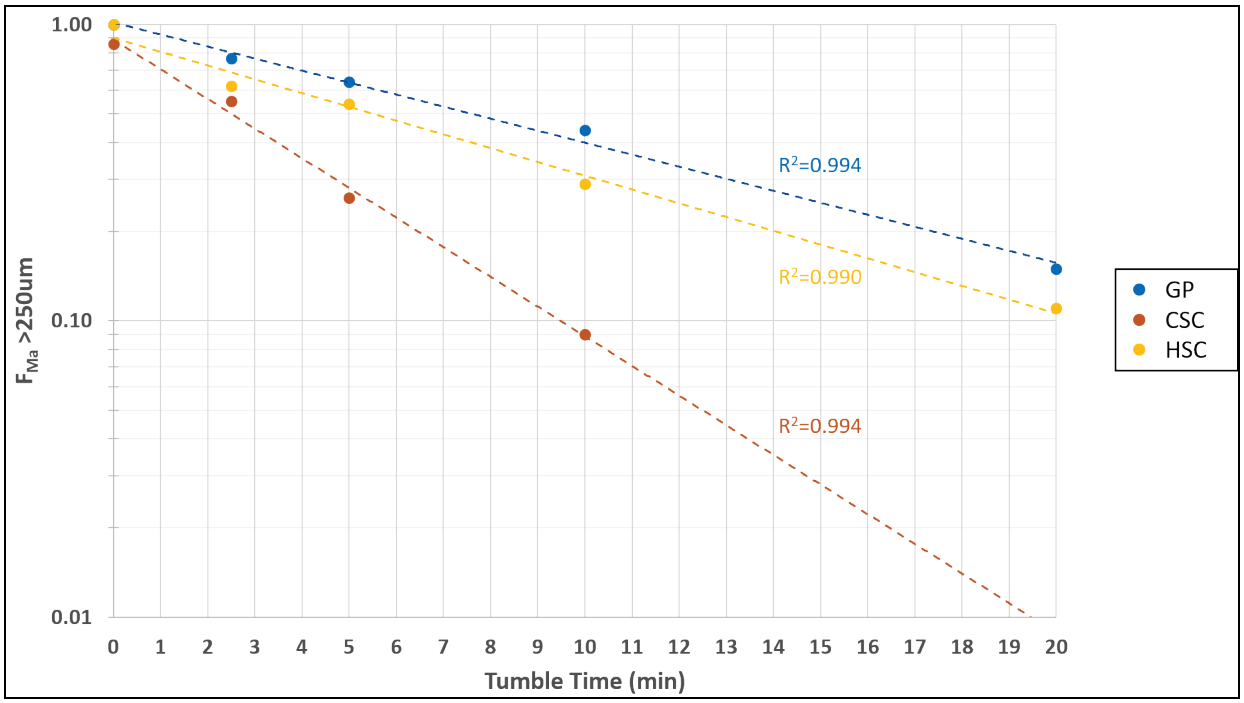

Table 6. Aggregate durability tumbling results. Water content of tumbled aggregates (w) and fraction >250 μm from wet sieve tests are presented along with tumbling abrasion rate (δ). * indicates samples with reduced w values for aggregate testing.

Sample Name	w	Wet Sieve (>250μm)	δ
DH	0.74	0.05	-0.195
ARE45	0.68*	0.01	-0.229
ARE60	0.25*	0.07	NA
SMIIL	1.02	0.04	-0.206
JR	1.20	0.03	-0.084
MS100	0.99	ND	-0.217
MS029	0.19	0.01	-0.042
MS021	0.18	0.02	-0.129
MS011	0.13	0.02	NA
MS003	0.19	0.02	NA
GP	1.96	ND	-0.093
CSC	1.27	0.14	-0.231
HSC	0.85*	ND	-0.107

While aggregate size was found to be strongly correlated with clay content, durability of aggregates was not. Figure 20 presents δ from the tumbling exponential decay models plotted against clay content. A statistically significant trend between these properties was not identified with R^2 =0.03 and p=0.63. Abrasion rates were similarly plotted against the other tested physical properties of the sediments and results of robust linear regression models are presented in Table 7. Only LOI was found to have a statistically significant correlation with δ, as seen in Figure 21. Despite the strong correlation shown in Figure 21, it is important to point out that MS029 and MS021 are not included in the model due to the absence of LOI data. However, inferences about the LOI of MS029 and MS021 can be made from the LOI of MS100. Since MS029 and MS021 were mixtures of laboratory test sand and naturally occurring sediment from the Mississippi River (MS100), nearly all organic material in the sediments would be expected to be associated with MS100. Therefore, it can estimated that the LOI% of these samples would be on the order of 29% and 21% of the MS100 LOI value. If accurate, this would result in LOI% values of 1.0 and 0.7 for MS029 and MS021, respectively. When plotted, these data group in the upper left corner of Figure 21, and remove statistical significance of the

regression model (R^2 =0.08, p=0.41). Regression plots between aggregate abrasion and the other physical parameters are presented in Appendix B.

Figure 20. Aggregate abrasion rate (δ) plotted against clay content. Solid line presents the robust linear regression best fit, with R^2 and p values provided. The dashed lines present the 95% confidence intervals of the fit.

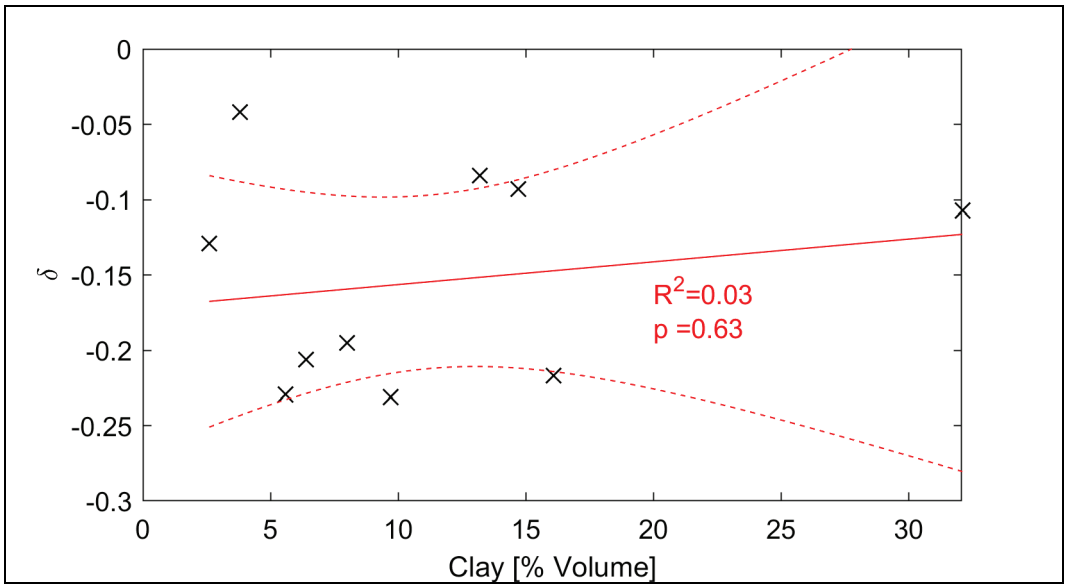

Table 7. Aggregate abrasion rate robust liner regression model outputs. Red font indicates variable p-values >0.05 and not statistically significant to the model.

Physical Parameter	R^2	p-value
%Clay	0.03	0.63
%Sand	0.02	0.37
w	<0.001	0.99
ρ	0.07	0.45
PI	0.04	0.53
ϕ_{sm}	0.06	0.50
LOI	0.89, 0.08*	$5.8x10^{-4}$, 0.41*

* Indicates the inclusion of MS029 and MS021 data.

Figure 21. Aggregate abrasion rate (δ) plotted against LOI. Solid line presents the robust linear regression best fit, with R^2 and p values provided. The dashed lines present the 95% confidence intervals of the fit. Red circles indicate estimated MS029 and MS021 data points.

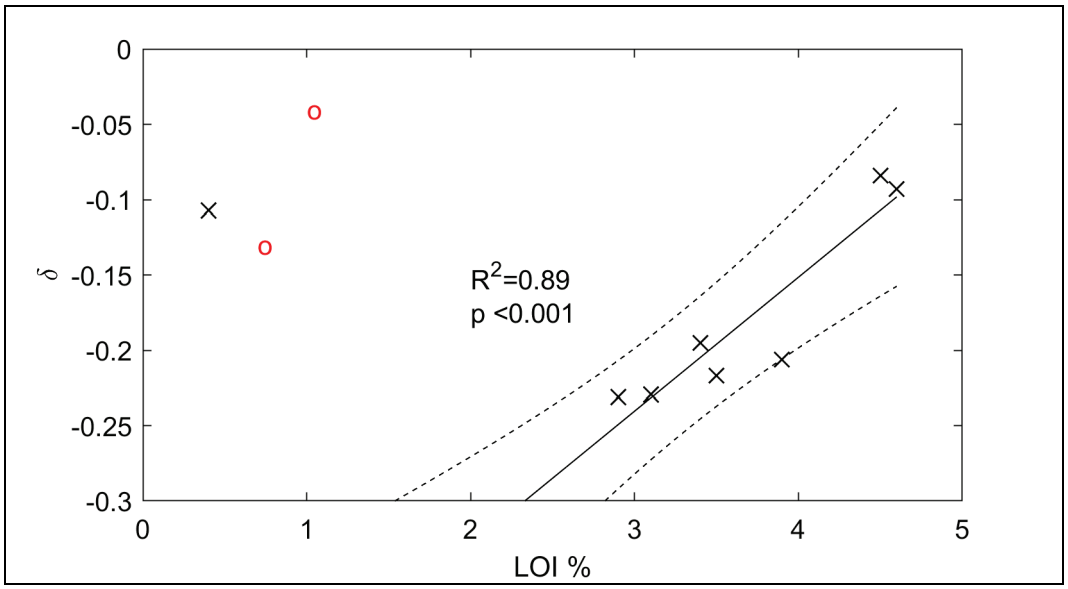

As with aggregate size, combinations of multivariate linear regression models were also run with the tested parameters. However, none of the multivariate regression models were found to be statistically significant. Tables of these regression model outputs can be found in Appendix B.

4 Summary, Conclusions and Recommendations

4.1 Summary and conclusions

To evaluate if commonly measured physical properties of sediment (grain size, density, water content, plasticity, volume fraction mud, and organic content) could be used to predict the production, size, and durability of muddy bed aggregates during erosion, a series of 13 sediments from USACE project locations across the country were examined. These sediments showed a wide range in physical parameters that have previously been linked to sediment cohesion (e.g. clay, organic content, w, plasticity, density, etc.), as shown in Table 2. Erosion testing indicated that the majority of the eroded volume occurred in the form of aggregated clasts >1000 μm for most sediment types evaluated (Figures 9-11; Table 3). Median grain size of eroded particles was found to be 10-450x larger than the median size of disaggregated samples for eleven of the test sediments (Table 3). Similar results for D_{50F}/D_{50L} ratios were observed in field erosion test studies conducted within the James River Estuary, where eroded sediment from muddy cores was 50-270x the median size of the disaggregated test bed (Perkey et al. 2020).

The D_{50F}/D_{50L} was found to have a strong positive correlation with clay content (Figure 15), and that aggregated clasts 10x the size of the disaggregated bed could be observed in sediments with clay contents as low as 2% (Table 3). Previously conducted studies have demonstrated that small amounts of clay (3-5%) can produce cohesive behavior and alter erosion processes of sediment (van Ledden 2004; Wu et al. 2018). Thus, the observation of aggregated bed clasts in low clay content sediment mixtures in this study aligns with previous work. Further, the data generated in this study suggest that aggregated mud clasts should be anticipated to occur as a result of bed erosion in sediment beds with clay contents adequate to produce cohesive behavior.

While not as strong as the relationship to clay content, significant correlations were also found between D_{50F}/D_{50L} and sand content, water content, and bulk density (Table 4). Weak, but significant correlations to these parameters were also identified in field cores collected throughout the James River Estuary (Perkey et al. 2020). Additionally, limited laboratory studies (e.g. Smith 1972; Jepsen et al. 2010) have documented

results that indicate both aggregate size and durability can be influenced by sand and water content. The Jepsen et al. (2010) study evaluated sediments from Boston Harbor, MA, Savannah Harbor, GA, and the Canaveral open water dredged material disposal area, FL, with an erosion flume and bedload trap. Their results indicated that the presence of muddy aggregates in the bedload trap decreased as sand content of the test sediments increased. Smith (1972) evaluated mud aggregates composed of three different sand mud mixtures with varying mineralogies and water contents. His results indicated that aggregates prepared from sediments with higher sand and lower water contents were less durable and resulted in smaller aggregated clasts after transport in flume testing. While these observations might be intuitive, it is important that the consistency of these trends be documented for the variety of test sediments that have been evaluated.

Though previous research has linked plasticity, organic content, and ϕ_{sm} with the cohesive nature of sediments (e.g. Jacobs et al. 2011; Dickhudt et al. 2009, 2011; Grant and Gust 1987; Yallop et al. 1994), these properties did not show significant correlation to the production and relative size of aggregated clasts observed in this study (Table 4). A multivariate regression model involving both PI and ϕ_{sm} was found to show significant correlation with D_{50F}/D_{50L} ratios, but this model was not as strong as the relationship observed with clay content alone. It is also important to point out that aggregated clasts were observed in sediments that did not display plastic behavior. Thus, using this property as a predictor of aggregate production and size is not recommended over clay content.

Durability testing of the aggregate cubes showed that abrasion of the clasts occurred rapidly and at rates that were best explained by exponential decay models. Only four of the test materials showed $F_{ma>250}$ greater than 0.10 following 20 min of tumbling (~200 m of linear distance). Despite the rapid rate of abrasion, these findings align with Sternberg's Law (Sternberg 1875), which relates pebble size to downstream transport distance through

$$D = D_o e^{-\delta L_t} \tag{5}$$

in which D_o is the particle diameter before transport, L_t is the length of travel, and δ is the abrasion rate. This suggests that commonly used

practices used to estimate the fining and break-up of gravel in streams may also be useful in estimating durability of eroded mud clasts.

Unlike bed aggregate size, aggregate abrasion rates were not found to correlate with contents of clay, sand, or water. Instead, a limited correlation with organic content through LOI measurements was identified (Table 7). This trend was only valid in muddy sediments and did not align with approximated LOI vales when plotted against abrasion rates from MS029 and MS021. It should be pointed out that the clay and organic content testing performed in this study did not provide information about the variety of clays or organic compounds present in the sediment. The impact these parameters have on sediment cohesion has been shown to vary with the specific nature of the clays (e.g. Mitchner and Torfs 1996; Barry et al 2006; Jacobs et al. 2011) or organic material (Grant and Gust 1987; Yallop et al. 1994). Thus, testing that evaluates the nature of the clays and organics present may be of more value than tests that simply measure abundance. Abundance testing was performed in this study due to the fact that these types of evaluations are more commonly used in characterizing sediments due to their lower cost.

It is important that the presence and transport characteristics of muddy bed aggregates be accounted for in models where transport dynamics are being simulated for cohesive sediments. Recent studies on muddy bed aggregates within the James River (Perkey and Smith 2019; Perkey et al. 2020) have highlighted the potential impact that aggregated clasts have on the transport pathways of fine sediment. Due to their size, eroded bed aggregates were predicted to have reduced time in a mobile state when compared to their constituent particles. Further, when bed aggregates were mobile, they were largely limited to bedload or insipient suspension, in contrast to smaller primary particles that were fully suspended within the water column. These same trends would be expected for the bed aggregates observed in this study, and thus impact the sediment transport processes within their respective environments.

The consistent observation of coarse-sand to gravel sized (>1000 μm) mud aggregates that are 10's-100'sx larger than their component particles based upon clay content provides guidance for size ranges of aggregated clasts produced following erosion of cohesive beds. Additionally, while tumbling testing performed in this study is not a direct simulation of bedload transport, it is reasonable to infer that the coarse mud aggregates would

likely degrade to smaller sized clasts during bedload transport, following exponential abrasion rates observed in this study. These trends may assist numerical modelers in developing sediment classifications representative of muddy bed aggregates for inclusion into numerical models as well as developing algorithms to describe their break-up and mass transfer to other sediment classes.

4.2 Recommendations

- Due to their abundant presence and impact on fine sediment transport pathways, it is recommended that numerical modeling in cohesive sediment environments incorporate particle classes that represent muddy bed aggregates.
- To incorporate these classes into model simulations, clay content in conjunction with the median disaggregated grain size could be used to estimate resultant bed aggregate sizes.
- While algorithms to address the weathering and breakdown of bed aggregates during transport do not currently exist within numerical model frameworks, in simulations where transport of sediment from a specified location is of focus (i.e. simulations evaluating dredge material placement areas) transport limits of bed aggregate classes could be set based upon break-up rates from tumbling tests.
- To develop algorithms that would represent the breakdown rate of muddy aggregates, further testing is needed to evaluate the durability and degradation processes of muddy bed aggregates in a more natural transport setting.

References

ASTM (ASTM International) D2216-19. 2019. *Standard Test Methods for Laboratory Determination of Water (Moisture) Content of Soil and Rock by Mass*. West Conshohocken, PA: ASTM International.

ASTM (ASTM International) D2974-14. 2014. *Standard Test Methods for Moisture, Ash, and Organic Matter of Peatand Other Organic Soils*. West Conshohocken, PA: ASTM International.

ASTM (ASTM International) D4318-05, 2015. *Standard Test Methods for Liquid Limit, Plastic Limit and Plasticity Index of Soils*. West Conshohocken, PA: ASTM International.

ASTM (ASTM International) D4644-87, 1998. *Standard Test Method for Slake Durability of Shales and Similar Weak Rocks*. West Conshohocken, PA: ASTM International.

ASTM (ASTM International) D6913-04. 2009. *Standard test methods for particle-size distribution (gradation) of soils using sieve analysis*. West Conshohocken, PA: ASTM International.

Barry, K. M., R. J. Thieke, and A. J. Mehta. 2006. "Quasi-Hydrodynamic Lubrication Effect of Clay Particles on Sand Grain Erosion." *Estuarine, Coastal and Shelf Science* 67(1-2): 161–169.

Brown, G. L., J. N. McAlpin, K. C. Pevey, P. V. Luong, C. R. Price, and B. A. Kleiss. 2019. *Mississippi River Hydrodynamic and Delta Management Study: Delta Management Modeling. AdH/SEDLIB Multi-Dimensional Model Validation and Scenario Analysis Report*. No. ERDC/CHL-TR-19-2. Vicksburg, MS: U.S. Army Engineer Research and Development Center. https://erdc-library.erdc.dren.mil/jspui/handle/11681/32446

Carey, D. A., K. Hickey, J.D. Germano, L.B. Read, M.E. Esten. 2013. Monitoring Survey at the Massachusetts Bay Disposal Site September/October 2013. DAMOS Contribution No. 195. U.S. Army Corps of Engineers, New England District, Concord, MA, 87 pp.

Delft Hydraulics. 2007. "User manual delft3d-flow: Wl." *Delft Hydraulics*.

Dickhudt, P. J., C. T. Friedrichs, L. C. Schaffner, and L. P. Sanford. 2009 "Spatial and temporal variation in cohesive sediment erodibility in the York River estuary, eastern USA: A biologically influenced equilibrium modified by seasonal deposition." *Marine Geology* 267, no. 3-4: 128-140.

Dickhudt, P. J., C. T. Friedrichs, and L. P. Sanford. 2011. "Mud matrix solids fraction and bed erodibility in the York River estuary, USA, and other muddy environments." *Continental Shelf Research* 31, no. 10: S3-S13.

Fall, K.A, D.W. Perkey, and S.J. Smith. 2020. "Characterization of Eroded Mud Aggregates with the Flume Imaging Camera System (FICS) and Its Added Value to Sediment Management Projects." ERDC/TN DOER-D22. Vicksburg, MS: U.S. Army Engineer Research and Development Center.

Fettweis, M., J. S. Houziaux, I. Du Four, V. Van Lancker, C. Baeteman, M. Mathys, D. Van den Eynde, F. Francken, and S. Wartel. 2009. "Long-Term Influence of Maritime Access Works on the Distribution of Cohesive Sediments: Analysis of Historical and Recent Data from the Belgian Nearshore Area (Southern North Sea)." *Geo-Marine Letters* 29(5): 321–330.

Grant, J., and G. Gust. 1987. "Prediction of coastal sediment stability from photopigment content of mats of purple sulphur bacteria." *Nature* 330, no. 6145: 244-246.

Jacobs, W., P. Le Hir, W. Van Kesteren, and P. Cann. 2011. "Erosion Threshold of Sand-Mud Mixtures." *Cont. Shelf Res.* 31, no.10 (S14–S25). doi:10.1016/j.csr.2010.05.012.

Jepsen, R., J. Roberts, and J. Gailani. 2010. "Effects of Bed Load and Suspended Load on Separation of Sands and Fines in Mixed Sediment." *J. Waterw. Port, Coast. Ocean Eng*. 136, no.6 : 319–326. https://doi.org/10.1061/(ASCE)WW.1943-5460.0000054.

Lesser, G. R., J. A. V. Roelvink, J. A. T. M. Van Kester, and G. S. Stelling. 2004. "Development and validation of a three-dimensional morphological model." *Coastal engineering* 51, no. 8-9: 883-915.

McNeil, J., C. Taylor, and W. Lick. 1996. "Measurements of erosion of undisturbed bottom sediments with depth." *Journal of Hydraulic Engineering* 122, no. 6: 316-324.

Mehta, A. J., E. J. Hayter, W. R. Parker, R. B. Krone, and A. M. Teeter. 1989. "Cohesive Sediment Transport. I: Process Description." *J. Hydraulic Eng*. 115(8): 1076–1093.

Mehta, A. J. 2013. *An introduction to hydraulics of fine sediment transport*. Vol. 38. World Scientific Publishing Company.

Perkey, D. W., and S. J. Smith. 2019. *Impact of Mud Aggregate Processes in Sediment Transport Studies*. ERDC/CHL CHETN-VIII-12. Vicksburg, MS: U.S. Army Engineer Research and Development Center. https://erdc-library.erdc.dren.mil/jspui/handle/11681/32005

Perkey, D. W., S. J. Smith, K. A. Fall, G. M. Massey, C. T. Friedrichs, and E. M. Hicks. 2020. "Impacts of Muddy Bed Aggregates on Sediment Transport and Management in the tidal James River, VA." *Journal of Waterway, Port, Coastal, and Ocean Engineering*. DOI: 10.1061/(ASCE)WW.1943-5460.0000578

Salehi, M. H., O. Hashemi Beni, H. Beigi Harchegani, I. Esfandiarpour Borujeni, and H. R. Motaghian. 2011. "Refining soil organic matter determination by loss-on-ignition." *Pedosphere* 21, no. 4: 473-482.

Schieber, J., J. B. Southard, and A. Schimmelmann. 2010. “Lenticular Shale Fabrics Resulting from Intermittent Erosion of Water-Rich Muds— Interpreting the Rock Record in the Light of Recent Flume Experiments.” *J. Sediment. Res.* 80, no.1 : 119–128. https://doi.org/10.2110/jsr.2010.005.

Schumacher, B. A. 2002. "Methods for the determination of total organic carbon (TOC) in soils and sediments." 1-23.

Smith, N. D. 1972. “Flume Experiments on the Durability of Mudclasts.” *SEPM Journal of Sedimentary Research* 42, no.2: 378–383.

Smith, S. J., and C. T. Friedrichs. 2011. “Size and Settling Velocities of Cohesive Flocs and Suspended Sediment Aggregates in a Trailing Suction Hopper Dredge Plume.” *Continental Shelf Research*. 31, no.10: S50-S63. doi:10.1016/j.csr.2010.04.002.

Sternberg, H. 1875. "Untersuchungen uber Langen-und Querprofil geschienbefuhrender Flusse.” Zeitschrift für Bauwesen, v. 25." 483-506.

Van Ledden, M., W. G. M. Van Kesteren, and J. C. Winterwerp. 2004. “A Conceptual Framework for the Erosion Behaviour of Sand-Mud Mixtures.” *Continental Shelf Research*. 24, no.1: 1–11. https://doi.org/10.1016/j.csr.2003.09.002.

Warner, J. C., C. R. Sherwood, R. P. Signell, C. K. Harris, and H. G. Arango. 2008. "Development of a three-dimensional, regional, coupled wave, current, and sediment-transport model." *Computers & Geosciences* 34, no. 10: 1284-1306.

Warner, J. C., B. Armstrong, R. He, and J. B. Zambon. 2010. "Development of a coupled ocean–atmosphere–wave–sediment transport (COAWST) modeling system." *Ocean modelling* 35, no. 3: 230-244.

Wentworth, C. K. 1929. "Method of computing mechanical composition types in sediments." *Bulletin of the Geological Society of America* 40, no. 4: 771-790.

Winterwerp, J. C., W. G. M. Van Kesteren, B. Van Prooijen, and W. Jacobs. 2012. "A conceptual framework for shear flow–induced erosion of soft cohesive sediment beds." *Journal of Geophysical Research: Oceans* 117, no. C10.

Wu, W., C. Perera, S. J. Smith, and A. Sanchez. 2018. "Critical shear stress for erosion of sand and mud mixtures." *Journal of Hydraulic Research* 56, no. 1: 96-110.

Yallop, M. L., B. de Winder, D. M. Paterson, and L. J. Stal. 1994. "Comparative structure, primary production and biogenic stabilization of cohesive and non-cohesive marine sediments inhabited by microphytobenthos." *Estuarine, Coastal and Shelf Science* 39, no. 6: 565-582.

Appendix A: D_{50F}/D_{50L} Linear Regression Model Results

This appendix presents plots and tables of the robust linear regression models between D_{50F}/D_{50L} and the physical parameters evaluated in this study. Plots of the single parameter regressions found to be statistically significant are presented first in black, followed by models with p-values >0.05, presented in red. Multi-parameter regression model outputs are then presented in a series of tables, corresponding to the number of parameters used in the regression.

Figure A1. Median particle size ratios plotted against clay content. Solid line presents the robust linear regression best fit, with R^2 and p values provided. The dashed lines present the 95% confidence intervals of the fit.

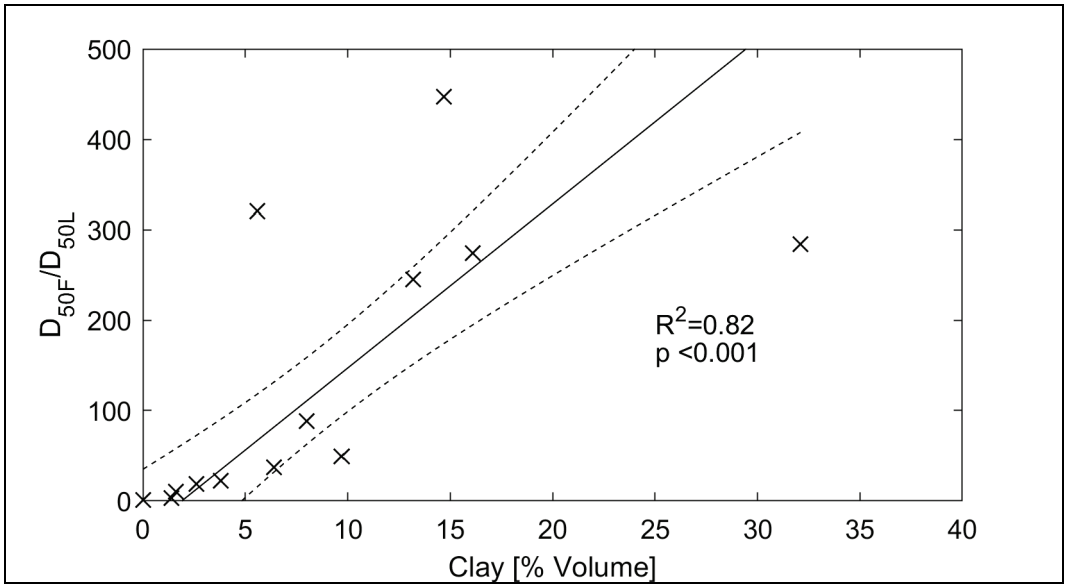

Figure A2. Median particle size ratios plotted against sand content. Solid line presents the robust linear regression best fit, with R^2 and p values provided. The dashed lines present the 95% confidence intervals of the fit.

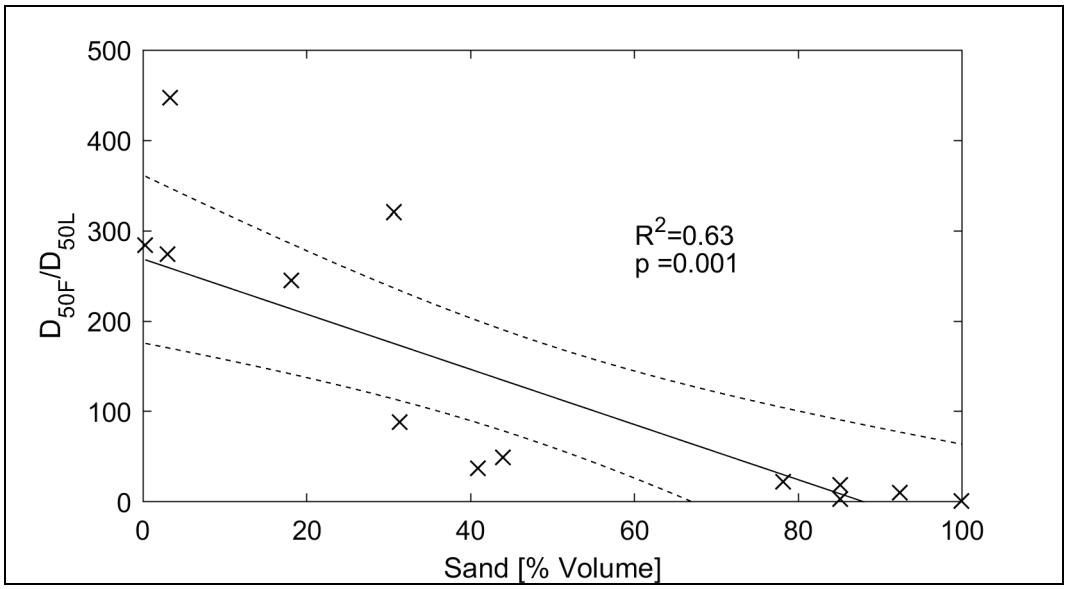

Figure A3. Median particle size ratios plotted against water content. Solid line presents the robust linear regression best fit, with R^2 and p values provided. The dashed lines present the 95% confidence intervals of the fit.

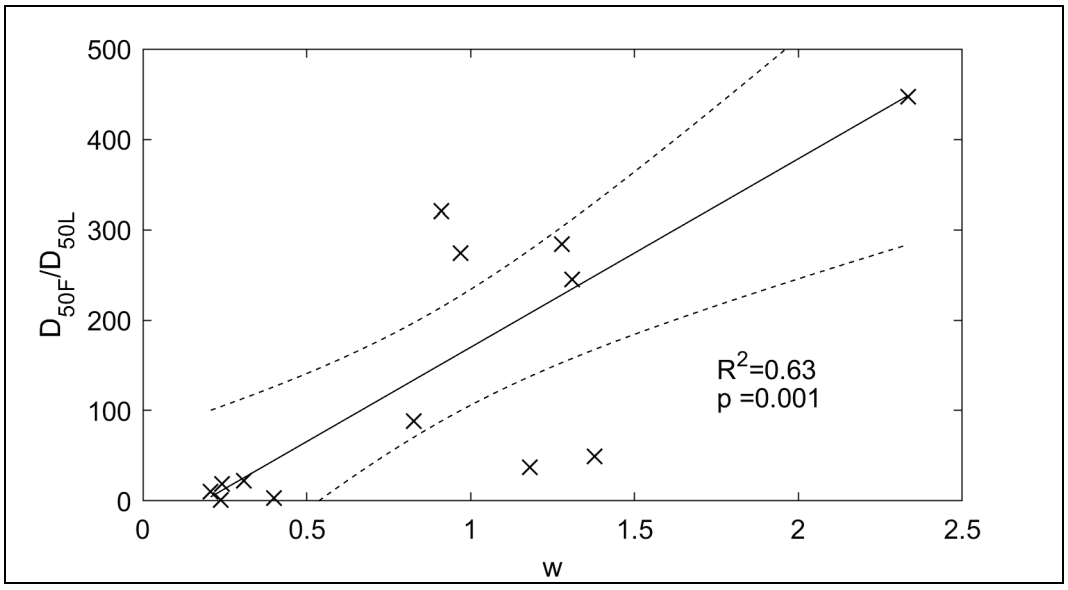

Figure A4. Median particle size ratios plotted against bulk density (ρ). Solid line presents the robust linear regression best fit, with R^2 and p values provided. The dashed lines present the 95% confidence intervals of the fit.

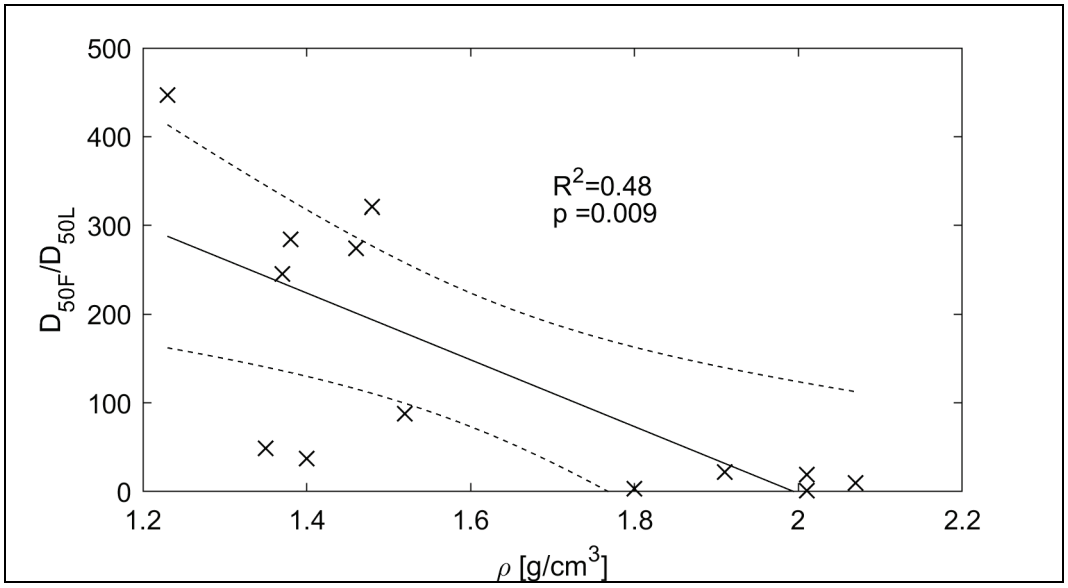

Figure A5. Median particle size ratios plotted against Plasticity Index (PI). Solid line presents the robust linear regression best fit, with R^2 and p values provided. The dashed lines present the 95% confidence intervals of the fit. Fit parameters are shown in red due to model p-values >0.05.

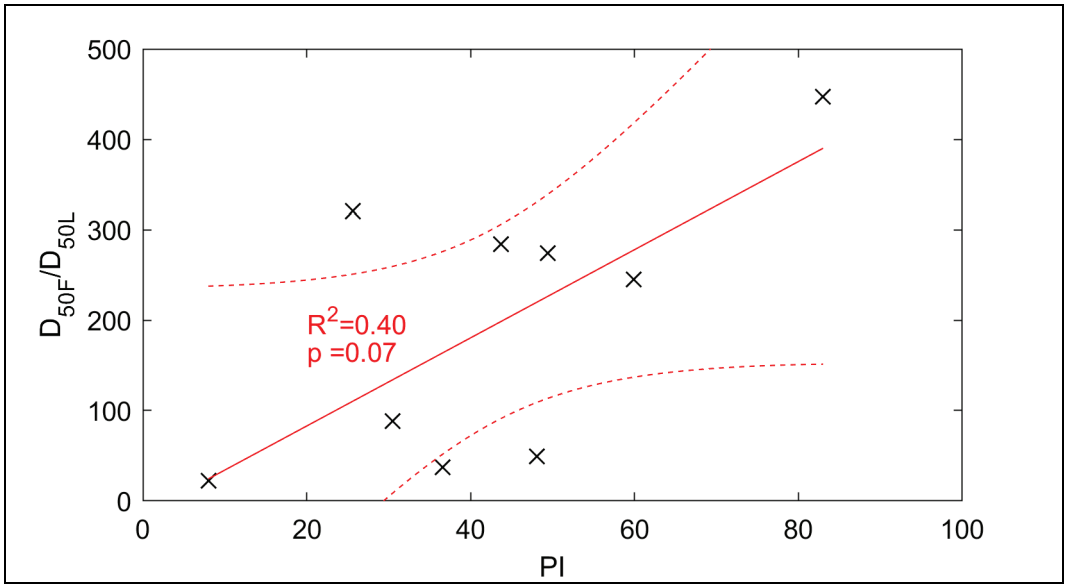

Figure A6. Median particle size ratios plotted against solid volume faction mud (ϕ_{sm}). Solid line presents the robust linear regression best fit, with R^2 and p values provided. The dashed lines present the 95% confidence intervals of the fit. Fit parameters are shown in red due to model p-values >0.05.

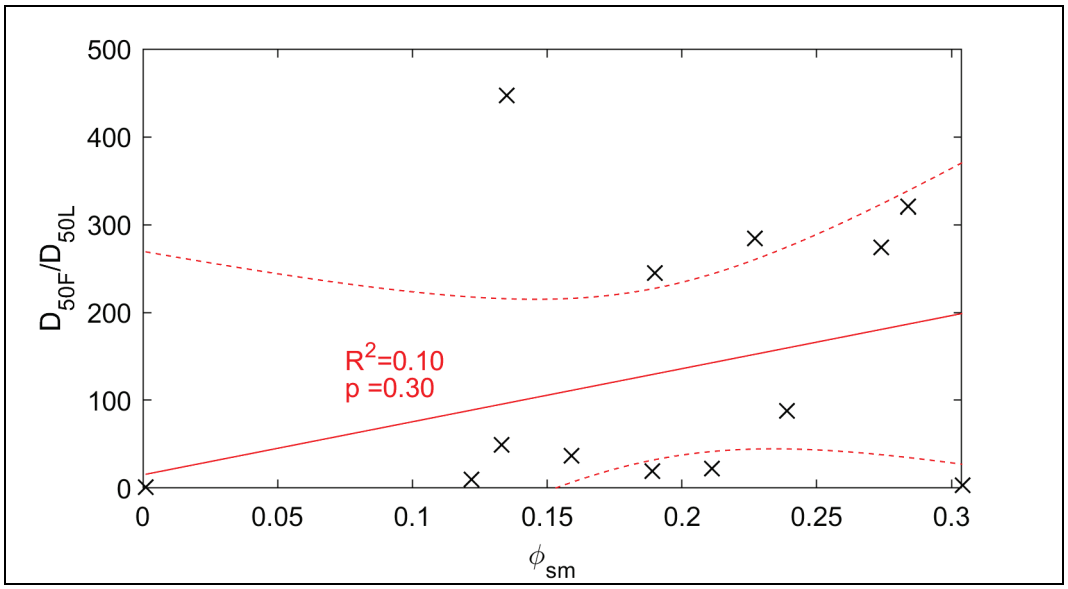

Figure A7. Median particle size ratios plotted against LOI. Solid line presents the robust linear regression best fit, with R^2 and p values provided. The dashed lines present the 95% confidence intervals of the fit. Fit parameters are shown in red due to model p-values >0.05.

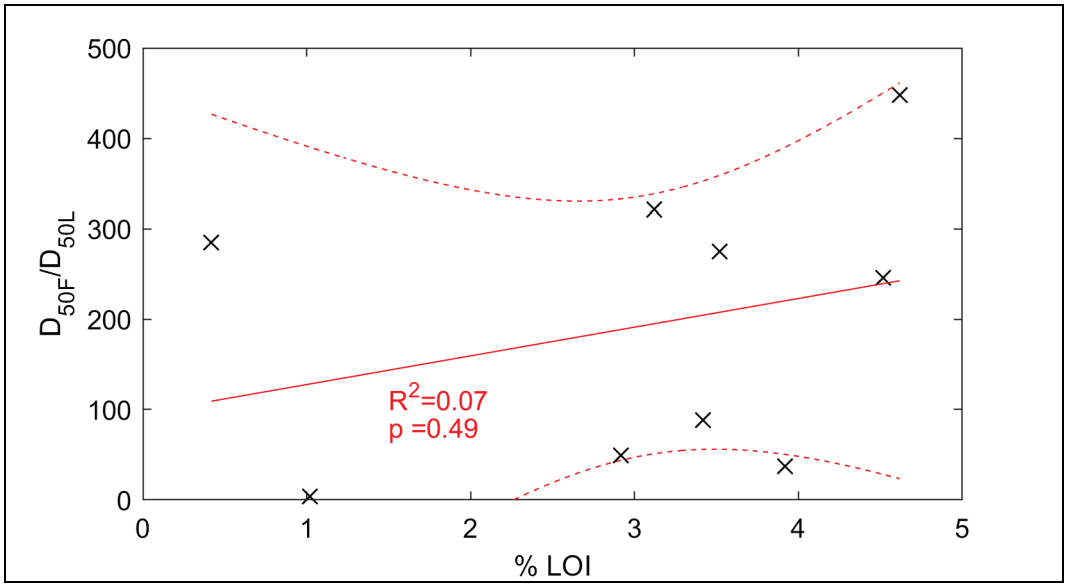

Table A1. D_{50F}/D_{50L} multiple linear regression model outputs (two parameters). Red font indicates variable p-values >0.05 and not statistically significant to the models.

Parameters	R^2	p-values	Parameter(s)	R^2	p-values
%Clay, %Sand	0.63	0.04, 0.95	%Sand, LOI	0.59	0.03, 0.89
%Clay, *w*	0.64	0.24, 0.04	*w*, PI	0.39	0.93, 0.56
%Clay, ρ	0.48	0.27, 0.23	*w*, ϕ_{sm}	0.62	0.003, 0.25
%Clay, PI	0.48	0.46, 0.15	*w*, LOI	0.37	0.14, 0.92
%Clay, ϕ_{sm}	0.47	0.02, 0.62	ρ, PI	0.41	0.27, 0.87
%Clay, LOI	0.44	0.09, 0.21	ρ, ϕ_{sm}	0.47	0.02, 0.75
%Sand, *w*	0.70	0.002, 0.08	ρ, LOI	0.31	0.20, 0.93
%Sand, ρ	0.71	0.013, 0.26	PI, ϕ_{sm}	0.7	0.01, 0.05
%Sand, PI	0.59	0.14, 0.72	PI, LOI	0.32	0.18, 0.64
%Sand, ϕ_{sm}	0.64	0.002, 0.89	ϕ_{sm}, LOI	0.08	0.82, 0.50

Table A2. D_{50F}/D_{50L} multiple linear regression model outputs (three parameters). Red font indicates variable p-values >0.05 and not statistically significant to the models.

Parameters	R^2	p-values	Parameter(s)	R^2	p-values
%Clay, %Sand, *w*	0.68	0.91, 0.17, 0.64	%Sand, *w*, ϕ_{sm}	0.69	0.17, 0.60, 0.92
%Clay, %Sand, ρ	0.71	0.58, 0.05, 0.35	%Sand, *w*, LOI	0.62	0.13, 0.56, 0.90
%Clay, %Sand, PI	0.62	0.68, 0.20, 0.83	%Sand, ρ, PI	0.69	0.11, 0.35, 0.30
%Clay, %Sand, ϕ_{sm}	0.68	0.79, 0.03, 0.80	%Sand, ρ, ϕ_{sm}	0.70	0.02, 0.29, 0.90
%Clay, %Sand, LOI	0.65	0.41, 0.15, 0.50	%Sand, ρ, LOI	0.60	0.12, 0.81, 0.83
%Clay, *w*, PI	0.46	0.51, 0.89, 0.69	%Sand, PI, ϕ_{sm}	0.71	0.92, 0.24, 0.24
%Clay, *w*, ϕ_{sm}	0.65	0.41, 0.04, 0.41	%Sand, PI, LOI	0.69	0.12, 0.79, 0.68
%Clay, *w*, LOI	0.49	0.34, 0.58, 0.60	%Sand, ϕ_{sm}, LOI	0.63	0.04, 0.53, 0.71
%Clay, ρ, PI	0.48	0.32, 0.94, 0.46	*w*, PI, ϕ_{sm}	**0.85**	0.09, 0.97, 0.01
%Clay, ρ, ϕ_{sm}	0.53	0.31, 0.20, 0.81	*w*, PI, LOI	0.31	0.99, 0.58, 0.69
%Clay, ρ, LOI	0.77	0.17, 0.20, 0.05	*w*, ϕ_{sm}, LOI	**0.91**	0.001, 0.003, 0.48
%Clay, PI, ϕ_{sm}	0.71	0.89, 0.04, 0.09	ρ, PI, ϕ_{sm}	0.72	0.82, 0.08, 0.07
%Clay, PI, LOI	0.37	0.64, 0.77, 0.79	ρ, PI, LOI	0.38	0.58, 0.29, 0.57
%Clay, ϕ_{sm}, LOI	0.53	0.08, 0.34, 0.15	ρ, ϕ_{sm}, LOI	**0.95**	0.001, 0.004, 0.40
%Sand, *w*, PI	0.63	0.15, 0.62, 0.77	PI, ϕ_{sm}, LOI	0.73	0.04, 0.07, 0.67

Table A3. D_{50F}/D_{50L} multiple linear regression model outputs (four variables). Red font indicates variable p-values >0.05 and not statistically significant to the models.

Parameters	R^2	p-values
%Clay, %Sand, *w*, PI	0.65	0.65, 0.21, 0.61, 0.71
%Clay, %Sand, *w*, ϕ_{sm}	0.70	0.91, 0.31, 0.63, 0.95
%Clay, %Sand, *w*, LOI	0.77	0.18, 0.09, 0.22, 0.20
%Clay, %Sand, ρ, PI	0.67	0.62, 0.18, 0.46, 0.52
%Clay, %Sand, ρ, ϕ_{sm}	0.73	0.52, 0.06, 0.33, 0.62
%Clay, %Sand, ρ, LOI	0.65	0.48, 0.20, 0.82, 0.57
%Clay, %Sand, PI, ϕ_{sm}	0.73	0.75, 0.75, 0.30, 0.31
%Clay, %Sand, PI, LOI	0.82	0.20, 0.07, 0.31, 0.29
%Clay, *w*, PI, ϕ_{sm}	0.86	0.99, 0.14, 0.97, 0.03
%Clay, *w*, PI, LOI	0.39	0.58, 0.69, 0.80, 0.66
%Clay, ρ, PI, ϕ_{sm}	0.72	0.88, 0.82, 0.13, 0.13
%Clay, ρ, PI, LOI	0.37	0.89, 0.80, 0.74, 0.98
%Sand, *w*, PI, ϕ_{sm}	0.89	0.36, 0.08, 0.55, 0.04
%Sand, *w*, PI, LOI	0.78	0.09, 0.29, 0.35, 0.37
%Sand, ρ, PI, ϕ_{sm}	0.71	0.95, 0.83, 0.30, 0.42
%Sand, ρ, PI, LOI	0.75	0.12, 0.36, 0.40, 0.33
%Sand, PI, ϕ_{sm}, LOI	0.72	0.94, 0.47, 0.46, 0.79
w, PI, ϕ_{sm}, LOI	0.96	0.03, 0.83, 0.01, 0.92
ρ, PI, ϕ_{sm}, LOI	0.95	0.04, 0.86, 0.01, 0.31

Table A4. D_{50F}/D_{50L} multiple linear regression model outputs (five parameters). Red font indicates variable p-values >0.05 and not statistically significant to the models.

Parameters	R^2	p-values
%Clay, %Sand, *w*, PI, ϕ_{sm}	0.96	0.12, 0.08, 0.03, 0.15, 0.02
%Clay, %Sand, *w*, PI, LOI	0.85	0.43, 0.13, 0.59, 0.94, 0.63
%Clay, %Sand, *w*, ϕ_{sm}, LOI	0.95	0.88, 0.61, 0.03, 0.06, 0.98
%Clay, %Sand, ρ, PI, ϕ_{sm}	0.72	0.82, 0.85, 0.97, 0.45, 0.56
%Clay, %Sand, ρ, PI, LOI	0.95	0.73, 0.04, 0.13, 0.84, 0.99
%Clay, %Sand, ρ, ϕ_{sm}, LOI	0.73	0.94, 0.94, 0.49, 0.51, 0.91
%Clay, %Sand, PI, ϕ_{sm}, LOI	0.82	0.41, 0.54, 0.61, 0.90, 0.41
%Clay, *w*, PI, ϕ_{sm}, LOI	0.95	0.96, 0.12, 0.97, 0.04, 0.94
%Clay, ρ, PI, ϕ_{sm}, LOI	0.95	0.73, 0.13, 0.84, 0.04, 0.99
%Sand, *w*, PI, ϕ_{sm}, LOI	0.96	0.74, 0.09, 0.71, 0.11, 0.82
%Sand, ρ, PI, ϕ_{sm}, LOI	0.94	0.97, 0.12, 0.92, 0.13, 0.59

Table A5. D_{50F}/D_{50L} multiple linear regression model outputs (six parameters). Red font indicates variable p-values >0.05 and not statistically significant to the models.

Parameters	R^2	p-values
%Clay, %Sand, *w*, PI, ϕ_{sm}, LOI	0.99	0.32, 0.31, 0.15, 0.84, 0.17, 0.36
%Clay, %Sand, ρ, PI, ϕ_{sm}, LOI	0.95	0.71, 0.75, 0.37, 0.97, 0.49, 0.87

Appendix B: Aggregate Abrasion Linear Regression Model Results

This appendix presents plots and tables of the robust linear regression models between aggregate abrasion and the physical parameters evaluated in this study. Plots of the single parameter regressions are presented first, multi-parameter regression model outputs are then presented in a series of tables, corresponding to the number of parameters used in the regression.

Figure B1. Aggregate abrasion rate (δ) plotted against sand content. Solid line presents the robust linear regression best fit, with R^2 and p values provided. The dashed lines present the 95% confidence intervals of the fit.

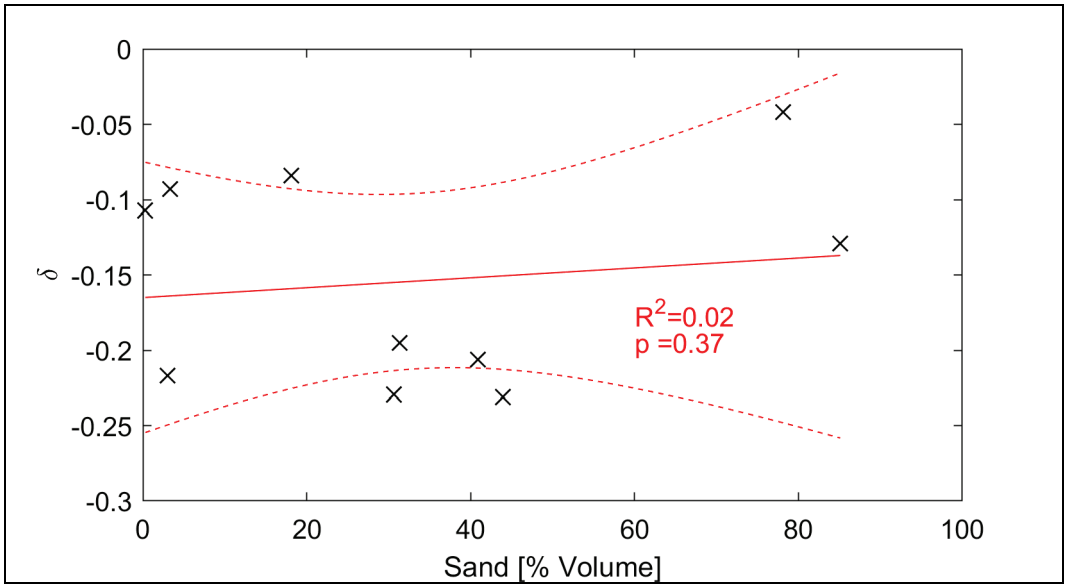

Figure B2. Aggregate abrasion rate (δ) plotted against water content (*w*). Solid line presents the robust linear regression best fit, with R^2 and p values provided. The dashed lines present the 95% confidence intervals of the fit.

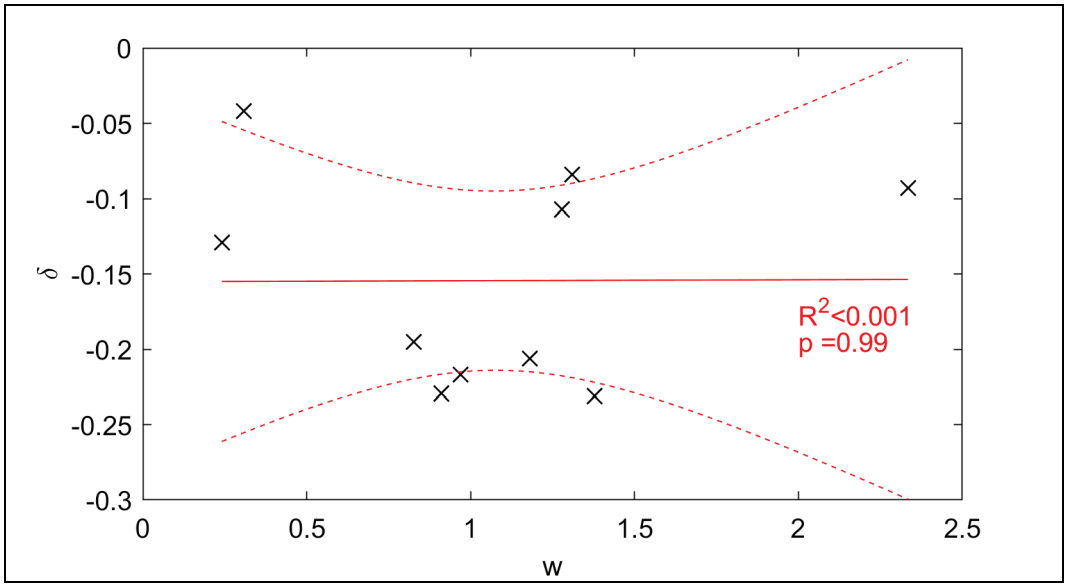

Figure B3. Aggregate abrasion rate (δ) plotted against bulk density (*ρ*). Solid line presents the robust linear regression best fit, with R^2 and p values provided. The dashed lines present the 95% confidence intervals of the fit.

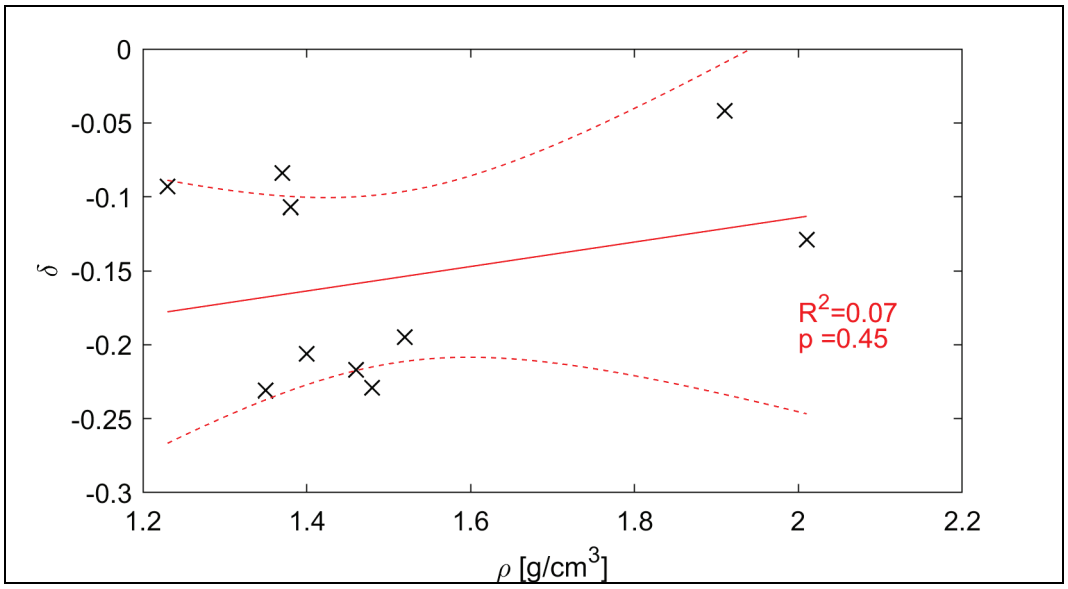

Figure B4. Aggregate abrasion rate (δ) plotted against plasticity index (PI). Solid line presents the robust linear regression best fit, with R^2 and p values provided. The dashed lines present the 95% confidence intervals of the fit.

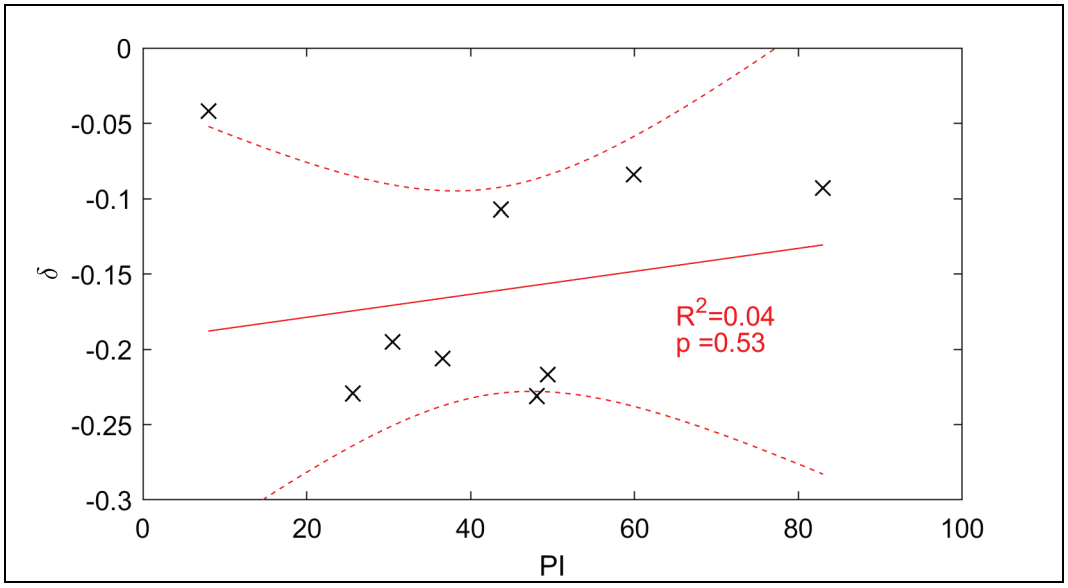

Figure B5. Aggregate abrasion rate (δ) plotted against solid volume fraction mud (ϕ_{sm}). Solid line presents the robust linear regression best fit, with R^2 and p values provided. The dashed lines present the 95% confidence intervals of the fit.

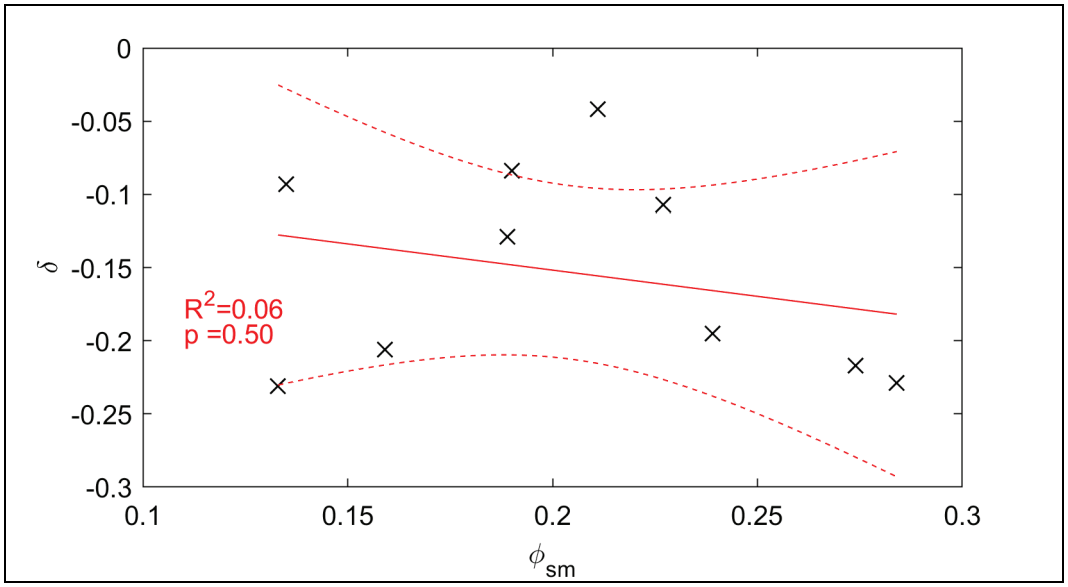

Table B1 Abrasion rate multiple linear regression model outputs (two parameters). Red font indicates variable p-values >0.05 and not statistically significant to the models.

Parameters	R^2	p-values	Parameter(s)	R^2	p-values
%Clay, %Sand	0.19	0.26, 0.27	%Sand, LOI	0.39	0.62, 0.14
%Clay, *w*	0.04	0.63, 0.80	*w*, PI	0.02	0.89, 0.81
%Clay, ρ	0.21	0.31, 0.24	*w*, ϕ_{sm}	0.06	0.77, 0.51
%Clay, PI	0.08	0.61, 0.88	*w*, LOI	0.31	0.81, 0.20
%Clay, ϕ_{sm}	0.10	0.59, 0.49	ρ, PI	0.50	0.05, 0.07
%Clay, LOI	0.69	0.02, 0.06	ρ, ϕ_{sm}	0.15	0.39, 0.44
%Sand, *w*	0.04	0.61, 0.70	ρ, LOI	0.32	0.88, 0.19
%Sand, ρ	0.12	0.59, 0.41	PI, ϕ_{sm}	0.05	0.90, 0.70
%Sand, PI	0.06	0.71, 0.58	PI, LOI	0.48	0.49, 0.08
%Sand, ϕ_{sm}	0.06	0.82, 0.58	ϕ_{sm}, LOI	0.08	0.96, 0.54

Table B2. Abrasion rate multiple linear regression model outputs (three parameters). Red font indicates variable p-values >0.05 and not statistically significant to the models.

Parameters	R^2	p-values	Parameter(s)	R^2	p-values
%Clay, %Sand, *w*	0.26	0.24, 0.23, 0.52	%Sand, *w*, LOI	0.54	0.29, 0.35, 0.98
%Clay, %Sand, ρ	0.23	0.39, 0.80,0.64	%Sand, ρ, PI	0.50	0.90, 0.89, 0.11
%Clay, %Sand, PI	0.32	0.23, 0.21, 0.35	%Sand, ρ, ϕ_{sm}	0.46	0.12, 0.08, 0.10
%Clay, %Sand, ϕ_{sm}	0.23	0.30, 0.33, 0.62	%Sand, ρ, LOI	0.56	0.23, 0.31, 0.89
%Clay, %Sand, LOI	0.68	0.15, 0.62, 0.14	%Sand, PI, ϕ_{sm}	0.06	0.81, 0.82, 0.99
%Clay, *w,* PI	0.05	0.68, 0.93, 0.92	%Sand, PI, LOI	0.54	0.58, 0.34, 0.79
%Clay, *w*, ϕ_{sm}	0.16	0.43, 0.47, 0.37	%Sand, ϕ_{sm}, LOI	0.60	0.09, 0.25, 0.90
%Clay, *w*, LOI	0.69	0.11, 0.63, 0.25	*w*, PI, ϕ_{sm}	0.07	0.73, 0.75, 0.61
%Clay, ρ, PI	0.60	0.33, 0.05, 0.09	*w*, PI, LOI	0.50	0.89, 0.36, 0.52
%Clay, ρ, ϕ_{sm}	0.37	0.21, 0.15, 0.27	*w*, ϕ_{sm}, LOI	0.38	0.24, 0.69, 0.80
%Clay, ρ, LOI	0.68	0.11, 0.69, 0.22	ρ, PI, ϕ_{sm}	0.52	0.08, 0.13, 0.66
%Clay, ϕ_{sm}, LOI	0.67	0.05, 0.71, 0.15	ρ, PI, LOI	0.49	0.85, 0.33, 0.52
%Sand, *w,* PI	0.07	0.62,0.82,0.67	ρ, ϕ_{sm}, LOI	0.40	0.22, 0.53, 0.98
%Sand, *w*, ϕ_{sm}	0.06	0.91, 0.84, 0.70	PI, ϕ_{sm}, LOI	0.50	0.14, 0.80, 0.54

Table B3. Abrasion rate multiple linear regression model outputs (four parameters). Red font indicates variable p-values >0.05 and not statistically significant to the models.

Parameters	R^2	p-values
%Clay, %Sand, *w*, PI	0.35	0.27, 0.25, 0.70, 0.48
%Clay, %Sand, *w*, ϕ_{sm}	0.26	0.30, 0.46, 0.65, 0.79
%Clay, %Sand, *w*, LOI	0.70	0.30, 0.70, 0.75, 0.34
%Clay, %Sand, ρ, PI	0.68	0.22, 0.40, 0.10, 0.08
%Clay, %Sand, ρ, ϕ_{sm}	0.47	0.80, 0.41, 0.20, 0.20
%Clay, %Sand, ρ, LOI	0.68	0.36, 0.75, 0.86, 0.37
%Clay, %Sand, PI, ϕ_{sm}	0.48	0.15, 0.19, 0.25, 0.36
%Clay, %Sand, PI, LOI	0.68	0.34, 0.66, 0.97, 0.42
%Clay, *w*, PI, ϕ_{sm}	0.17	0.54, 0.69, 0.84, 0.50
%Clay, *w*, PI, LOI	0.75	0.19, 0.40, 0.47, 0.28
%Clay, ρ, PI, ϕ_{sm}	0.68	0.24, 0.06, 0.19, 0.39
%Clay, ρ, PI, LOI	0.72	0.23, 0.48, 0.55, 0.32
%Sand, *w*, PI, ϕ_{sm}	0.07	0.91, 0.80, 0.77, 0.88
%Sand, *w*, PI, LOI	0.54	0.63, 0.89, 0.80, 0.88
%Sand, ρ, PI, ϕ_{sm}	0.65	0.30, 0.06, 0.78, 0.27
%Sand, ρ, PI, LOI	0.55	0.60, 0.77, 0.99, 0.96
%Sand, PI, ϕ_{sm}, LOI	0.60	0.47, 0.79, 0.56, 0.79
w, PI, ϕ_{sm}, LOI	0.50	0.99, 0.48, 0.85, 0.61
ρ, PI, ϕ_{sm}, LOI	0.50	0.98, 0.53, 0.88, 0.68

Table B4. Abrasion rate multiple linear regression model outputs (five parameters). Red font indicates variable p-values >0.05 and not statistically significant to the models.

Parameters	R^2	p-values
%Clay, %Sand, *w*, PI, ϕ_{sm}	0.48	0.23, 0.28, 0.85, 0.35, 0.46
%Clay, %Sand, *w*, PI, LOI	0.77	0.30, 0.64, 0.48, 0.51, 0.34
%Clay, %Sand, *w*, ϕ_{sm}, LOI	0.87	0.18, 0.24, 0.24, 0.26, 0.18
%Clay, %Sand, ρ, PI, ϕ_{sm}	0.68	0.65, 0.98, 0.27, 0.62, 0.81
%Clay, %Sand, ρ, PI, LOI	0.67	0.56, 0.95, 0.93, 0.93, 0.55
%Clay, %Sand, ρ, ϕ_{sm}, LOI	0.70	0.48, 0.70, 0.74, 0.76, 0.48
%Clay, %Sand, PI, ϕ_{sm}, LOI	0.67	0.56, 0.95, 0.93, 0.93, 0.55
%Clay, *w*, PI, ϕ_{sm}, LOI	0.75	0.30, 0.57, 0.54, 0.81, 0.38
%Clay, ρ, PI, ϕ_{sm}, LOI	0.71	0.36, 0.69, 0.66, 0.98, 0.45
%Sand, *w*, PI, ϕ_{sm}, LOI	0.60	0.57, 0.98, 0.86, 0.66, 0.84
%Sand, ρ, PI, ϕ_{sm}, LOI	0.59	0.57, 0.94, 0.83, 0.69, 0.83

Table B5. Abrasion rate multiple linear regression model outputs (six parameters). Red font indicates variable p-values >0.05 and not statistically significant to the models.

Parameters	R^2	p-values
%Clay, %Sand, *w*, PI, ϕ_{sm}, LOI	0.91	0.31, 0.41, 0.36, 0.60, 0.44, 0.31
%Clay, %Sand, ρ, PI, ϕ_{sm}, LOI	0.68	0.66, 0.90, 0.79, 0.86, 0.91, 0.65

Unit Conversion Factors

Multiply	By	To Obtain
microns	1.0 E-06	meters

Acronyms

USACE	U.S. Army Corps of Engineers
FICS	Flume Imaging Camera System
ERDC-CHL	Engineer Research and Development Center-Coastal and Hydraulics Laboratory
LRE	USACE Detroit District
LRB	USACE Buffalo District
NAP	USACE Philadelphia District
SMIIL	Seven Mile Island Living Laboratory
NAO	USACE Norfolk District
MVN	USACE New Orleans District
CSC	Calcasieu Shipping Channel
RSM	Regional sediment management
SWG	USACE Galveston District
PI	Plasticity Index
LOI	loss on ignition
LDPSA	Laser Diffraction Particle Size Analysis
esd	equivalent spherical diameters
HSC	Houston Ship Channel
GP	Gulfport entrance channel

REPORT DOCUMENTATION PAGE

Form Approved
OMB No. 0704-0188

1. REPORT DATE *(DD-MM-YYYY)*	2. REPORT TYPE	3. DATES COVERED *(From - To)*
September 2020	Final	

4. TITLE AND SUBTITLE

Physical Factors That Influence Muddy Bed Aggregate Production, Size, and Durability

5a. CONTRACT NUMBER

5b. GRANT NUMBER

5c. PROGRAM ELEMENT NUMBER

6. AUTHOR(S)

David W. Perkey, Kelsey A. Fall, and S. Jarrell Smith

5d. PROJECT NUMBER

5e. TASK NUMBER

5f. WORK UNIT NUMBER

7. PERFORMING ORGANIZATION NAME(S) AND ADDRESS(ES)

Coastal and Hydraulics Laboratory
U.S. Army Engineer Research and Development Center
3909 Halls Ferry Road
Vicksburg, MS 39180-6199

8. PERFORMING ORGANIZATION REPORT NUMBER

ERDC/CHL TR-20-19

9. SPONSORING / MONITORING AGENCY NAME(S) AND ADDRESS(ES)

The Regional Sediment Management Program (RSM) and the Dredging Operations and Environmental Research Program (DOER) Vicksburg, MS 39180

10. SPONSOR/MONITOR'S ACRONYM(S)

11. SPONSOR/MONITOR'S REPORT NUMBER(S)

12. DISTRIBUTION / AVAILABILITY STATEMENT

Approved for public release; distribution is unlimited.

13. SUPPLEMENTARY NOTES

RSM: "James River Federal Navigation Channel, Lower Reaches" – Account Code D15945 AMSCO 008303
DOER: "Aggregate Transport" – Account Code B3209G AMSCO 089500

14. ABSTRACT

Aggregation state significantly influences the transport characteristics of fine sediments. While research has documented the presence of mud aggregates in multiple coastal and estuarine environments, bed aggregates are largely absent from numerical models used to predict cohesive sediment transport. The U.S. Army Corps of Engineers (USACE) is conducting studies to evaluate the impact muddy bed aggregates have on sediment management issues, and how to account for aggregates in numerical models.

In this study, physical properties associated with cohesive behavior were evaluated to determine if they could be used as predictors for bed aggregate production, size, and durability. Results showed that aggregates were consistently produced in cohesive sediments, and that median aggregate size was ~10-450x larger than the disaggregated sediment. Clay content had strong correlation with relative aggregate size, though statistically significant correlations were also found with sand content, water content, and density. Durability testing indicated that aggregate break-up followed exponential models, and that in limited instances, rates of break-up correlated with organic content.

15. SUBJECT TERMS

Sediment transport--Numerical analysis
Cohesive sediments
Suspended sediments
Bed load
Soil structure

16. SECURITY CLASSIFICATION OF:			17. LIMITATION OF ABSTRACT	18. NUMBER OF PAGES	19a. NAME OF RESPONSIBLE PERSON
a. REPORT	b. ABSTRACT	c. THIS PAGE			19b. TELEPHONE NUMBER *(include area code)*
Unclassified	Unclassified	Unclassified	SAR	65	